

UCSF

UC San Francisco Previously Published Works

Title

Systematic characterization of gene function in a photosynthetic organism

Permalink

<https://escholarship.org/uc/item/8j40v8dn>

Authors

Vilarrasa-Blasi, Josep
Fauser, Friedrich
Onishi, Masayuki
[et al.](#)

Publication Date

2020-12-11

DOI

10.1101/2020.12.11.420950

1 **Systematic characterization of gene function in a photosynthetic organism**

2

3 Josep Vilarrasa-Blasi^{4,6,*}, Friedrich Fauser^{1,4,*}, Masayuki Onishi^{5,7}, Silvia Ramundo⁸, Weronika
4 Patena^{1,4}, Matthew Millican⁴, Jacqueline Osaki⁴, Charlotte Philp⁴, Matthew Nemeth⁴, Patrice A.
5 Salomé⁹, Xiaobo Li^{1,4,14}, Setsuko Wakao^{10,11}, Rick G. Kim⁴, Yuval Kaye⁴, Arthur R. Grossman⁴,
6 Krishna K. Niyogi^{10,11,12}, Sabeeha Merchant^{9,13}, Sean Cutler³, Peter Walter⁸, José R. Dinneny^{4,6,☒},
7 Martin C. Jonikas^{1,4,☒} and Robert E. Jinkerson^{2,3,4,☒}

8

9 ¹Department of Molecular Biology, Princeton University, Princeton, NJ, USA.

10 ²Department of Chemical and Environmental Engineering, University of California, Riverside,
11 CA, USA.

12 ³Department of Botany and Plant Sciences, University of California, Riverside, CA, USA.

13 ⁴Department of Plant Biology, Carnegie Institution for Science, Stanford, CA, USA.

14 ⁵Department of Biology, Duke University, Durham, NC, USA.

15 ⁶Department of Biology, Stanford University, Stanford, CA, USA.

16 ⁷Department of Genetics, Stanford University School of Medicine, Stanford, CA, USA.

17 ⁸Department of Biochemistry and Biophysics, University of California, San Francisco, CA, USA.

18 ⁹Department of Chemistry and Biochemistry and Institute for Genomics and Proteomics,
19 University of California, Los Angeles, CA, USA.

20 ¹⁰Department of Plant and Microbial Biology, University of California, Berkeley, CA 94720, USA.

21 ¹¹Molecular Biophysics and Integrated Bioimaging Division, Lawrence Berkeley National
22 Laboratory, Berkeley, CA 94720, USA.

23 ¹²Howard Hughes Medical Institute, University of California, Berkeley, CA 94720, USA.

24 ¹³Department of Molecular and Cell Biology, University of California, Berkeley, CA, USA.

25

26 * These authors contributed equally to this work

27 ☒ e-mail: dinneny@stanford.edu, mjonikas@princeton.edu, robert.jinkerson@ucr.edu

28

29 ¹⁴Present address: Life Sciences, Westlake University, Hangzhou, Zhejiang Province, China

30 **Photosynthetic organisms are essential for human life, yet most of their genes remain**
31 **functionally uncharacterized. Single-celled photosynthetic model systems have the potential**
32 **to accelerate our ability to connect genes to functions. Here, using a barcoded mutant library**
33 **of the model eukaryotic alga *Chlamydomonas reinhardtii*, we determined the phenotypes of**
34 **more than 58,000 mutants under more than 121 different environmental growth conditions**
35 **and chemical treatments. 78% of genes are represented by at least one mutant that showed**
36 **a phenotype, providing clues to the functions of thousands of genes. Mutant phenotypic**
37 **profiles allow us to place known and previously uncharacterized genes into functional**
38 **pathways such as DNA repair, photosynthesis, the CO₂-concentrating mechanism, and**
39 **ciliogenesis. We illustrate the value of this resource by validating novel phenotypes and gene**
40 **functions, including the discovery of three novel components of a defense pathway that**
41 **counteracts actin cytoskeleton inhibitors released by other organisms. The data also inform**
42 **phenotype discovery in land plants: mutants in *Arabidopsis thaliana* genes exhibit similar**
43 **phenotypes to those we observed in their *Chlamydomonas* homologs. We anticipate that this**
44 **resource will guide the functional characterization of genes across the tree of life.**

45 Major contributions to our understanding of gene functions in photosynthetic organisms
46 have been made by studying microbial models, including the discovery and characterization of the
47 Calvin-Benson-Bassham CO₂ fixation cycle¹ as well as the structures², order³ and cloning⁴ of
48 complexes in the photosynthetic electron transport chain. Advances in technology now provide
49 opportunities for microbes to serve as powerful complements to land plants in the characterization
50 of gene functions by enabling significantly higher experimental throughput⁵.

51 The single-celled green alga *Chlamydomonas* (*Chlamydomonas reinhardtii*) is a well-
52 established model system for studies of key pathways including photosynthesis, primary

53 metabolism, inter-organelle communication, and stress response⁶. Furthermore, amenability to
54 microscopy and biochemical purifications have made *Chlamydomonas* a leading model system for
55 studies of cilia⁷⁻⁹. Despite promising progress with the development of clustered regularly
56 interspaced short palindromic repeats (CRISPR)-based reagents to generate targeted mutants^{10,11},
57 low editing efficiencies currently prevent large scale CRISPR sgRNA library screens in
58 *Chlamydomonas*. The recent generation of a barcoded *Chlamydomonas* mutant collection
59 facilitates the study of individual genes and enables forward genetic screens¹². In the present work,
60 we leverage the amenability of *Chlamydomonas* for high-throughput methods to connect
61 genotypes to phenotypes on a massive scale, allowing placement of genes into pathways and
62 discovery of conserved gene functions in land plants.

63

64 **Systematic genome-scale phenotyping**

65 To connect genotypes to phenotypes, we measured the growth of 58,101 *Chlamydomonas*
66 mutants representing 14,695 genes (83% of all genes encoded in the *Chlamydomonas* genome,
67 based on the current genome annotation, v5.6) under 121 environmental and chemical stress
68 conditions (both control and experimental conditions are given in Table S1 and Table S2). We
69 pooled the entire *Chlamydomonas* mutant collection and used molecular barcodes to quantify the
70 relative abundance of each mutant after competitive growth (Fig. 1a-f). Growth conditions
71 included heterotrophic, mixotrophic, and photoautotrophic growth under different photon flux
72 densities and CO₂ concentrations, as well as abiotic stress conditions such as various pH and
73 temperatures. We also subjected the library to known chemical stressors, including DNA
74 damaging agents, reactive oxygen species, antimicrobial drugs such as paromomycin and
75 spectinomycin, as well as the actin-depolymerizing drug latrunculin B (LatB). To further expand

76 our knowledge of chemical stressors in photosynthetic organisms, we identified 1,222 small
77 molecules from the Library of AcTive Compounds on Arabidopsis (LATCA)¹³ that negatively
78 influence *Chlamydomonas* growth (Extended Data Fig. 1, Table S3, Extended Data File 1), and
79 performed competitive growth experiments in the presence of 52 of the most potent compounds.
80 Taken together, this effort represents, to the best of our knowledge, the largest genotype-by-
81 phenotype dataset to date for any photosynthetic organism, with 62 million data points (Table S4).

82

83 **Mutants show genotype-phenotype specificity and enrichment of expected functions**

84 To identify mutants with growth defects or enhancements due to a specific treatment, we
85 compared the abundance of each mutant after growth under the treatment condition to its
86 abundance after growth under a control condition (Fig. 2a). We called this comparison a screen,
87 and the ratio of these abundances the mutant phenotype (Fig. 2b,c). Mutant phenotypes were
88 reproducible between independent replicates of a screen (Fig. 2c,d).

89 Individual mutants exhibited genotype-phenotype specificity. For example, mutants
90 disrupted in the DNA repair gene *POLYMERASE ZETA* (*POLZ*, encoded by Cre09.g387400)
91 exhibited growth defects in the presence of the DNA crosslinker cisplatin, and these mutants did
92 not show growth defects in unrelated screens (Fig. 2d). We observed similar genotype-phenotype
93 specificity for other genes and phenotypes including sensitivity to low CO₂, ciliogenesis, and
94 latrunculin B (LatB) sensitivity (Fig. 2d).

95 In many screens, mutants that exhibited phenotypes were enriched for disruptions in genes
96 with expected function. 46 out of 223 screens, show at least one enriched (FDR <0.05) Gene
97 Ontology (GO)¹⁴ term associated with mutants (Fig. 2e, Extended Data Fig. 2, Table S5). These
98 enriched GO terms corresponded to functions known to be required for survival under the

99 respective treatments. For example, screens with DNA-damaging agents resulted in GO term
100 enrichments such as “DNA replication,” “Nucleotide binding,” or “Damaged DNA binding.”
101 These GO term enrichments suggest that the phenotypic screens are correctly identifying genes
102 required for growth under the corresponding stresses.

103 13,840 genes (78% of all *Chlamydomonas* genes) are represented by one or more mutant
104 alleles that showed a phenotype (decreased abundance below our detection limit) in at least one
105 screen. While a lone mutant showing a phenotype is not sufficient evidence to conclusively
106 establish a gene-phenotype relationship, we anticipate that these data will be useful to the research
107 community in at least three ways: first, they can help prioritize the characterization of candidate
108 genes identified by other means, such as transcriptomics or protein-protein interactions. Second,
109 they facilitate the generation of hypotheses about the functions of poorly-characterized genes.
110 Third, they enable prioritization of available mutant alleles for further study. The genotype-
111 phenotype specificity of individual mutants and the enrichment of expected functions suggest that
112 our data can serve as a guide for understanding the functions of thousands of poorly-characterized
113 genes.

114

115 **High-confidence, novel gene-phenotype relationships**

116 The availability of multiple independent mutant alleles for individual genes allowed us to
117 identify high-confidence gene-phenotype relationships. When multiple independent mutant alleles
118 for the same gene show the same phenotype, the confidence in a gene lesion-phenotype
119 relationship increases because it is less likely that the phenotype is due to a mutation elsewhere in
120 the genome, or that there was an error in mapping of the mutation¹². Using a statistical framework
121 that leverages multiple independent mutations in the same gene (see Methods), we identified 1,636

122 high-confidence (FDR <0.3) gene-phenotype relationships involving 684 genes (Fig. 3a, Table S6,
123 Table S7), including hundreds of genes with no functional annotation.

124 As an example of how individual gene-phenotype relationships advance our understanding,
125 we made the unexpected observation that mutants in the gene encoding the chloroplast unfolded
126 protein response (cpUPR) kinase, MUTANT AFFECTED IN CHLOROPLAST-TO-NUCLEUS
127 RETROGRADE SIGNALING (*MARS1*)¹⁷, were sensitive (FDR <10⁻⁹) to the DNA damaging
128 agent methyl methanesulfonate (MMS) (Fig. 3b). We validated this phenotype in a separate growth
129 assay and showed that the MMS sensitivity of these mutants is rescued by complementation with
130 a wild-type copy of *MARS1* but not by a kinase-dead version (Fig. 3c-d). We also determined that
131 treatment with MMS leads to induction of VESICLE-INDUCING PROTEIN IN PLASTIDS 2
132 (*VIPP2*), a highly selective cpUPR marker, in wild-type cells but not in mutants lacking *MARS1*
133 (Fig. 3e). These results illustrate the value of our high-throughput data and suggest the intriguing
134 possibility that the cpUPR is activated via *MARS1* upon DNA damage or protein alkylation and
135 has a protective role against these stressors.

136

137 **From phenotypes to pathways**

138 To facilitate data visualization and to help the prediction of functions for poorly-
139 characterized genes in our dataset, we used the principle that genes whose mutants have similar
140 phenotypes tend to function in the same pathway⁵. We clustered the 684 genes with high-
141 confidence phenotypes based on the similarity of their phenotypes across different treatments (Fig.
142 4a and Extended Data File 2). The correlation of phenotypes was largely unrelated to
143 transcriptional expression correlation, suggesting that the two approaches provide complementary
144 information (Extended Data Fig. 3, Table S8). We named some of our gene clusters based on the

145 presence of previously characterized genes or based on the conditions that produced the most
146 dramatic phenotypes in a cluster (Fig. 4b-g). Below, we provide examples of how the data
147 recapitulate known genetic relationships and provide insights into the functions of poorly
148 characterized genes.

149

150 **Essential DNA repair pathways are conserved to green algae**

151 DNA damage repair pathways are among the best-characterized and most highly conserved
152 across all organisms^{19,20}, thus, they serve as a useful test case of the quality of our data. In our
153 dataset, 21 homologues of known DNA repair proteins formed a large cluster (Fig. 4e),
154 demonstrating the quality of our phenotypic data, validating our ability to identify that these genes
155 work in a common pathway, and extending the conservation of their functions to green algae.

156 Mutants for various DNA repair genes exhibit expected differences in their sensitivities to
157 different types of DNA damage: 1) DNA double-strand breaks (zeocin and bleomycin), 2) DNA
158 crosslinks (Mitomycin C and cisplatin), and 3) DNA alkylation (MMS). For example, mutants
159 exhibiting sensitivity to all DNA damage conditions included cells lacking upstream DNA
160 damage-sensing kinase ATAXIA TELANGIECTASIA AND RAD3-related protein (ATR,
161 encoded by Cre10.g467200)²¹; as well as mutants lacking the cell cycle checkpoint control protein
162 RADIATION SENSITIVE 9 (RAD9, encoded by Cre16.g682950) or its binding partner
163 HYDROXYUREA-SENSITIVE 1 (HUS1, encoded by Cre12.g524350)²². Mutants specifically
164 sensitive to the double-strand break-inducing agents zeocin and bleomycin included the upstream
165 sensor of double-strand breaks, the kinase ATAXIA-TELANGIECTASIA MUTATED (ATM,
166 encoded by Cre13.g564350)²³ (Table S6); as well as DNA POLYMERASE THETA (POLQ,
167 encoded by Cre16.g664301), which facilitates error-prone double-strand break repair and can

168 maintain genome integrity when other repair pathways are insufficient^{24,25} (Table S6). Mutants
169 specifically sensitive to the DNA crosslinker cisplatin included cells with genetic lesions in the
170 helicases REGULATOR OF TELOMERE ELONGATION HELICASE 1 (RTEL1, encoded by
171 Cre02.g089608)²⁶, in FANCONI ANEMIA COMPLEMENTATION GROUP M (FANCM,
172 encoded by Cre03.g208833), and in the crossover junction endonuclease METHANSULFONATE
173 UV SENSITIVE 81 (MUS81, encoded by Cre12.g555050).

174 Our data suggest several instances where a given factor is required for the repair of a
175 specific kind of DNA damage in *Chlamydomonas* but not in *Arabidopsis*, or vice-versa, suggesting
176 lineage-specific differences in how DNA damage is repaired. For example, *Chlamydomonas*
177 *fancm* mutants are sensitive to the DNA crosslinker cisplatin, while *Arabidopsis fancm* mutants
178 are not²⁷. Conversely, *Arabidopsis mus81* mutants are sensitive to the alkylating agent MMS and
179 the DNA crosslinker Mitomycin C²⁸, while *Chlamydomonas mus81* mutants were not.

180 Taken together, our data suggest that the core eukaryotic DNA repair machinery defined
181 in other systems is generally conserved in green algae. Moreover, the observation of expected
182 phenotypes illustrates the quality of the presented data and the utility of the platform for chemical
183 genomic studies.

184

185 **The data allow classification of photosynthesis genes**

186 Our data allowed the classification of 38 genes whose disruption leads to a
187 photoautotrophic growth defect¹² into two clusters. One cluster consisted of genes whose
188 disruption confers sensitivity to light when grown on medium supplemented with acetate while
189 the other contained genes whose disruption does not (Fig. 4b-c, Extended Data File 2).

190 The light-sensitive cluster (Fig. 4c) included genes encoding core photosynthesis
191 components and biogenesis factors such as the pmRNA trans-splicing factors *RNA MATURATION*
192 *Of PSAA (RAA1)*²⁹, *RAA3*³⁰, *OCTOTRICOPEPTIDE REPEAT 120 (OPR120)*, and *OPR104*³¹;
193 Photosystem II biogenesis factor *CONSERVED IN PLANT LINEAGE AND DIATOMS 10*
194 *(CPLD10)*^{31,32} the chlorophyll biogenesis factor *Mg-CHELATASE SUBUNIT D (CHLD)*³³; the
195 ATP synthase translation factor *TRANSLATION DEFICINET ATPase 1 (TDA1)*³⁴; the Rubisco
196 mRNA stabilization factor *MATURATION OF RBCL 1 (MRL1)*³⁵; and the Calvin-Benson-
197 Bassham cycle enzymes *SEDOHEPTULOSE-BISPHOSPHATASE 1 (SEBPI)*³⁶ and
198 *PHOSPHORIBULOKINASE 1 (PRK1)*³⁷. Several highly conserved but poorly characterized genes
199 are also found in this cluster, including the putative Rubisco methyltransferase Cre12.g524500³⁸,
200 the putative thioredoxins Cre01.g037800, Cre06.g281800, and Cre13.g572100; as well as four
201 *Chlorophyta*-specific genes. The mutant phenotypes of these poorly-characterized genes and their
202 presence in this light-sensitive cluster together suggest that their products could mediate the
203 biogenesis, function, or regulation of core components of the photosynthetic machinery.

204 The light-insensitive cluster (Fig. 4b) contained known and novel components of the algal
205 CO₂-concentrating mechanism (CCM), as detailed below.

206

207 **Novel CO₂-concentrating mechanism components**

208 The CO₂-concentrating mechanism increases the CO₂ concentration around the CO₂ fixing
209 enzyme Rubisco, thus enhancing the rate of carbon uptake. The mechanism uses carbonic
210 anhydrases in the chloroplast stroma to convert CO₂ to HCO₃⁻, which is transported into the lumen
211 of the thylakoid membranes that traverse a Rubisco-containing structure called the pyrenoid³⁹.
212 There, the lower pH drives the conversion of HCO₃⁻ back into concentrated CO₂ that feeds

213 Rubisco³⁹. Mutants deficient in the CO₂-concentrating mechanism are unable to grow
214 photoautotrophically in air, but their photoautotrophic growth is rescued in 3% CO₂³⁹. We
215 observed this phenotype for one or more alleles of genes whose disruption was previously shown
216 to disrupt the CCM (Table S4), including genes encoding the chloroplast envelope HCO₃⁻
217 transporter LOW CO₂ INDUCIBLE GENE A (LCIA)⁴⁰, and the thylakoid lumen CARBONIC
218 ANHYDRASE 3 (CAH3)⁴¹, the stromal carbonic anhydrase LOW CO₂ INDUCIBLE GENE B
219 (LCIB)⁴², the master transcriptional regulator CCM1/CIA5^{43,44}, and the pyrenoid structural protein
220 STARCH GRANULES ABNORMAL 1 (SAGA1)⁴⁵(Table S6).

221 Similarly, we observed high CO₂ rescue of photoautotrophic growth defects for mutants in
222 multiple poorly characterized genes in the light-insensitive cluster, suggesting that many of these
223 genes are novel components in the CO₂-concentrating mechanism. These genes formed a cluster
224 with *SAGA1*⁴⁵, the only previously known CO₂-concentrating mechanism gene with enough alleles
225 to be present in the cluster. We named one of these components, Cre06.g259100, *SAGA3* because
226 its protein product shows homology to the two pyrenoid structural proteins SAGA1 and SAGA2⁴⁶
227 (Extended Data Fig. 4). Consistent with a role in the CO₂-concentrating mechanism, *SAGA3*
228 localizes to the pyrenoid⁴⁷. We also observed this phenotype in mutants lacking the pyrenoid starch
229 sheath-localized *STARCH BRANCHING ENZYME 3 (SBE3)*⁴⁸, suggesting that this enzyme plays
230 a key role in the biogenesis of the pyrenoid starch sheath, a structure surrounding the pyrenoid that
231 has recently been shown to be important for pyrenoid function under some conditions⁴⁹. Our
232 cluster also contains FUZZY ONIONS (FZO)-like (FZL), a dynamin-related membrane
233 remodeling protein involved in thylakoid fusion and light stress; mutants in this gene have
234 pyrenoid shape defects⁵⁰. Our results suggest that thylakoid organization influences pyrenoid
235 function. Additional genes showing similar phenotypes included *CLVI* (encoded by

236 Cre13.g574000), a predicted voltage-gated chloride channel that we hypothesize is important for
237 regulating the ion balance in support of the CO₂-concentrating mechanism, or alternatively, may
238 directly mediate HCO₃⁻ transport; a protein containing a Rubisco-binding motif (encoded by
239 Cre12.g528300); and a predicted Ser-Thr kinase (Cre02.g111550). The kinase is a promising
240 candidate for a regulator in the CO₂-concentrating mechanism, as multiple CCM components are
241 known to be phosphorylated⁵¹⁻⁵³, but no kinase had previously been shown to have a CCM
242 phenotype.

243 Also in this cluster of high CO₂ rescue genes are the predicted *PYRUVATE*
244 *DEHYDROGENASE 2 (PDH2)* (Cre03.g194200) and the predicted *DIHYDROLIPOYL*
245 *DEHYDROGENASE (DLD2)* (Cre01.g016514). We hypothesize that these proteins are part of a
246 glycine decarboxylase complex that functions in photorespiration, a pathway that recovers carbon
247 from the products of the Rubisco oxygenation reaction. *PDH2* was found in the pyrenoid
248 proteome⁵⁴, suggesting the intriguing possibility that glycine decarboxylation may be localized to
249 the pyrenoid, where the recovered CO₂ could be captured by Rubisco.

250

251 **Novel genes with roles in cilia function**

252 Chlamydomonas cells swim using two motile cilia. To identify mutants with abnormal cilia
253 function, we separated mutants based on swimming ability by placing the pool of mutants in a
254 vertical column and collecting the supernatant and pellet. In this assay, mutants with altered
255 swimming behavior were enriched in GO terms such as “dynein complex,” which comprises motor
256 proteins involved in ciliary motility (Fig. 2e). 18 genes were represented by enough alleles to
257 provide high confidence (FDR < 0.3) that their disruption produces a defect in swimming (Fig.
258 4d). These genes were enriched ($P=0.0075$, Fisher’s exact test) in genes encoding proteins found

259 in the *Chlamydomonas* flagella proteome⁵⁵. Half of these genes or their orthologs have previously
260 been associated with a cilia-related phenotype in *Chlamydomonas* and/or mice (Table S9).

261 In our analysis, these 18 genes formed four clusters that appeared to sub-classify their
262 function (Fig. 4d). The first cluster is enriched in known regulators of ciliary membrane
263 composition and includes *NEPHROCYSTIN-4-LIKE PROTEIN (NPHP4)*⁵⁶; its physical interactor
264 *TRANSMEMBRANE PROTEIN 67 (TMEM67, also named MECKEL SYNDROME TYPE 3*
265 *[MKS3]* in mammals), which has been implicated in photoreceptor intraciliary transport⁵⁷; and
266 *CENTRIOLE PROTEOME PROTEIN 290 (CEP290)*⁵⁸. We validated the swimming defect of
267 *tmem67* and observed that the mutant has shorter cilia (Extended Data Fig. 5). The poorly-
268 annotated gene Cre15.g638551 clusters with these genes, suggesting that it may also regulate
269 ciliary membrane composition.

270 The second cluster contains *BARDET-BIEDL SYNDROME 1 PROTEIN 1 (BBS1)* and
271 *BBS9*, components of the Bardet-Biedl syndrome-associated complex that regulates targeting of
272 proteins to cilia⁵⁹. The poorly annotated gene Cre15.g640502 clustered with these genes,
273 suggesting that it may also play a role in targeting proteins to cilia.

274 The third cluster contains eight genes, four of which relate to the dynein complex. These
275 genes include the ciliary dynein assembly factor *DYNEIN ASSEMBLY LEUCINE-RICH REPEAT*
276 *PROTEIN (DAU1)*^{60,61}; *OUTER DYNEIN ARM (ODA)*; *DYNEIN ARM INTERMEDIATE CHAIN*
277 *1 (DIC1)*⁶²; *DYNEIN HEAVY CHAIN 1 (DHC1)*⁶³; and *TUBULIN-TYROSINE LIGASE 9,*
278 *(TLL9)*, which modulates ciliary beating through the addition of a polyglutamate chains to alpha
279 tubulin⁶⁴. The predicted thioredoxin peroxidase gene Cre04.g218750 and three poorly annotated
280 genes (Cre07.g338850, Cre01.g012900, and Cre16.g675600) clustered with these genes,
281 suggesting possible roles in dynein assembly or regulation.

282 The fourth cluster contains three poorly characterized genes, *FLAGELLA ASSOCIATED*
283 *PROTEIN2 (FAP2)*, *FLAGELLA ASSOCIATED PROTEIN 81 (FAP81)*, and *TEF24*. The protein
284 encoded by FAP81 (Cre06.g296850) was identified in the *Chlamydomonas* cilia proteome⁵⁵, and
285 its human homolog DELETED IN LUNG AND ESOPHAGEAL CANCER PROTEIN 1 (*DLECI*)
286 localizes to motile cilia⁶⁵. We validated the swimming defect of the *fap81* mutant and established
287 that it has shorter cilia (Extended Data Fig. 5). The localization to motile cilia in humans and our
288 finding that mutating the encoding gene leads to a ciliary motility defect together suggests the
289 intriguing possibility that impaired cilia motility contributes to certain lung and esophageal
290 cancers.

291

292 **Novel genes required for actin cytoskeleton integrity**

293 Our analysis revealed a group of genes whose mutation render cells sensitive to LatB (Fig.
294 4g). LatB binds to monomers of actin, one of the most abundant and conserved proteins in
295 eukaryotic cells, and prevents actin polymerization⁶⁶ (Fig. 5a). LatB was first discovered as a small
296 molecule that protects the sea sponge *Latrunculina magnifica* from predation by fish⁶⁷, and is an
297 example of the chemical warfare that organisms use to defend themselves and compete in nature
298 (Fig. 5b).

299 *Chlamydomonas* protects itself against LatB-mediated inhibition of its conventional actin
300 INNER DYNEIN ARM5 (*IDA5*) by upregulating the highly divergent actin homologue NOVEL
301 ACTIN-LIKE PROTEIN1 (*NAP1*), which appears to perform most of the same functions as actin
302 but is resistant to inhibition by LatB⁶⁸. Upon inhibition of *IDA5* by LatB, *IDA5* is degraded and
303 divergent actin *NAP1* is expressed⁶⁸. The expression of *NAP1* is dependent on three other known

304 genes, *LatB-SENSITIVE (LAT1-LAT3)* (Fig. 5c); thus, mutants lacking any of these four genes are
305 highly sensitive to LatB⁶⁸.

306 Our phenotype data revealed three novel components of this F-actin homeostasis pathway,
307 which we named LAT5 (Cre17.g721950), LAT6 (Cre15.g640101) and LAT7 (Cre11.g482750).
308 LAT5 and LAT6 clustered together with three previously known components of the pathway:
309 *NAP1*, *LAT2* and *LAT3*; and disruption of all six genes rendered cells sensitive to LatB (Table S6).
310 Mutants in all three novel components show a relatively mild phenotype when compared with
311 those mutants in *LAT1-LAT3* (Fig. 5d), illustrating the sensitivity of our phenotyping platform.

312 Ubiquitin proteasome-mediated proteolysis of IDA5 has been hypothesized to drive the
313 degradation of IDA5 and promote the formation of F-NAP1⁶⁹, but the factors involved were
314 unknown. *LAT5* and *LAT6* encode predicted subunits of a SKP1, CDC53/CULLIN, F-BOX
315 RECEPTOR (SCF) E3 ubiquitin ligase, whose homologs promote the degradation of target
316 proteins⁷⁰ the disruption of *LAT5* and *LAT6* impaired degradation of IDA5 upon LatB treatment,
317 suggesting that LAT5 and LAT6 mediate IDA5 degradation (Fig. 5e). *LAT7* encodes a predicted
318 importin, and its disruption impairs NAP1 accumulation after LatB treatment (Fig. 5e), suggesting
319 that nuclear import is required for NAP1 biosynthesis.

320 It was previously not clear how broadly conserved this F-actin homeostasis pathway is. We
321 found that the land plant model Arabidopsis has homologs of IDA5, NAP1, LAT3, LAT5, LAT6
322 and LAT7. We observed that Arabidopsis mutants disrupted in *LAT3*, *LAT5*, and *LAT6* are
323 sensitive to LatB treatment (Fig. 5f-g), which was not expected *a priori*, suggesting that this
324 pathway for actin cytoskeleton integrity and the gene functions identified here are conserved in
325 land plants.

326 **Discussion**

327 In this work, we determined the phenotypes of 58,101 *Chlamydomonas* mutants across a broad
328 variety of growth conditions. We observed a phenotype for mutants representing 13,840 genes,
329 providing a valuable starting point for characterizing the functions of thousands of genes. Mutant
330 phenotypes are searchable at chlamylibrary.org, and individual mutants can be ordered from the
331 *Chlamydomonas* Resource Center.

332 We provided several examples of how the data enable discovery of novel gene functions
333 and phenotypes in algae and plants. We validated our discovery of three novel genes in the actin
334 cytoskeleton integrity pathway, obtained insights into their molecular functions, and found that
335 this pathway appears to be conserved in land plants. We validated our discovery of cilia function
336 defects for two novel genes and our observation of an unexpected sensitivity of the chloroplast
337 unfolded protein response to the alkylating agent MMS. We also discussed how our data provide
338 insights and candidate genes in other pathways including DNA damage repair, photosynthesis, and
339 the CO₂ concentrating mechanism.

340 This work illustrates the value of using a microbial photosynthetic organism for
341 discovering novel gene functions on a large scale. We hope that the genotype-phenotype
342 relationships identified here will guide the characterization of thousands of genes, with potential
343 applications in agriculture, the global carbon cycle, and our basic understanding of cell biology.

344 **Acknowledgments**

345 We thank Matthew Cahn for developing and improving the CLiP website; Xuhuai Ji at the Stanford
346 Functional Genomics Facility and Ziming Weng at the Stanford Center for Genomics and
347 Personalized Medicine for deep sequencing services; Kathryn Barton, Winslow Briggs, and Zhi-
348 Yong Wang for providing lab space; Ted Raab for providing lab equipment; Jacob Robertson and
349 Nina Ivanova for helping with library maintenance; Members of the Dinneny, Jonikas, and
350 Jinkerson Labs, Tingting Xiang, and Alexandra Wilson for constructive suggestions on the
351 manuscript.

352 This project was supported by grants from the National Institutes of Health (DP2-GM-
353 119137), the National Science Foundation (MCB-1914989 and MCB-1146621), and the Simons
354 Foundation and Howard Hughes Medical Institute (55108535) awarded to M.C.J.; a German
355 Academic Exchange Service (DAAD) research fellowship awarded to F.F.; Simons Foundation
356 fellowships of the Life Sciences Research Foundation awarded to R.E.J. and J.V.-B.; EMBO long
357 term fellowship (ALTF 1450-2014 and ALTF 563-2013) awarded to J.V.-B and S.R.; an NSF
358 MCB Grant (1818383) awarded to M.O.; and a Swiss National Science Foundation Advanced
359 PostDoc Mobility Fellowship (P2GEP3_148531) awarded to S.R; a Simons Foundation and
360 Howard Hughes Medical Institute (55108515) Faculty Scholars grant awarded to J.R.D. Work in
361 the Merchant laboratory is supported by a cooperative agreement with the US Department of
362 Energy Office of Science, Office of Biological and Environmental Research program under Award
363 DE-FC02-02ER63421.

364 **Author Contributions**

365 S.W. and K.K.N. performed rose bengal treatments; R.G.K., Y.K., and A.R.G. performed
366 anoxia and high light treatments; J.V.-B., F.F., and R.E.J. prepared mutant pools, performed all
367 other treatments, and processed all samples; S.C. provided the LATCA compounds; M.M., J.O.,
368 C.P., and M.N. validated the active LATCA compounds; M.M. performed chemoinformatics
369 analysis; M.O. validated LatB phenotypes in *Chlamydomonas* and performed immunoblots; S.R.
370 and P.W. validated the *mars1* phenotype; W.P. guided statistical analysis and website
371 development; P.A.S. and S.M. provided transcriptomics data; X.L. provided early access to the
372 *Chlamydomonas* mutant library; J.V.-B. and J.R.D. confirmed *Arabidopsis* phenotypes; J.V.-B.,
373 F.F., M.C.J., and R.E.J. designed experiments, analyzed, and interpreted the data; J.V.-B., F.F.,
374 M.C.J., and R.E.J. wrote the manuscript with input from all authors.

375

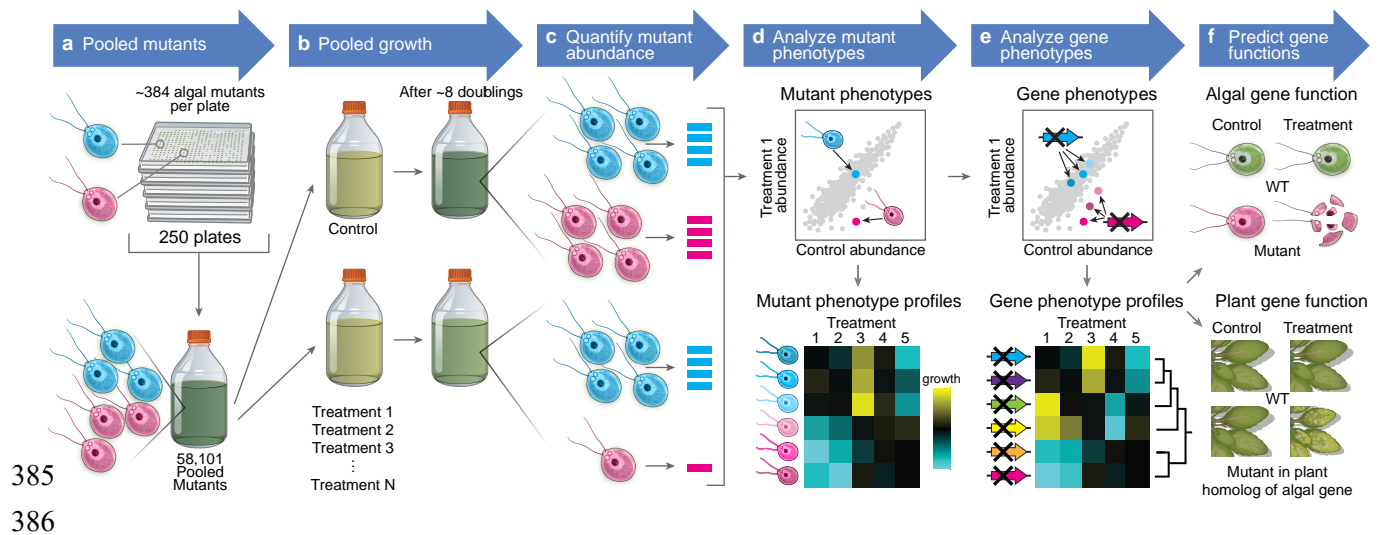
376 The authors declare no competing financial interests. J.V.-B., F.F., M.C.J., and R.E.J. wish to note
377 that a provisional patent application on aspects of the findings has been submitted.

378

379 **Additional Information**

380 Supplementary information is available for this paper. J.V.B and F.F. contributed equally to this
381 work. Correspondence and requests for materials should be addressed to J.D.
382 (dinney@stanford.edu), M.C.J. (mjonikas@princeton.edu) and R.E.J.
383 (robert.jinkerson@ucr.edu).

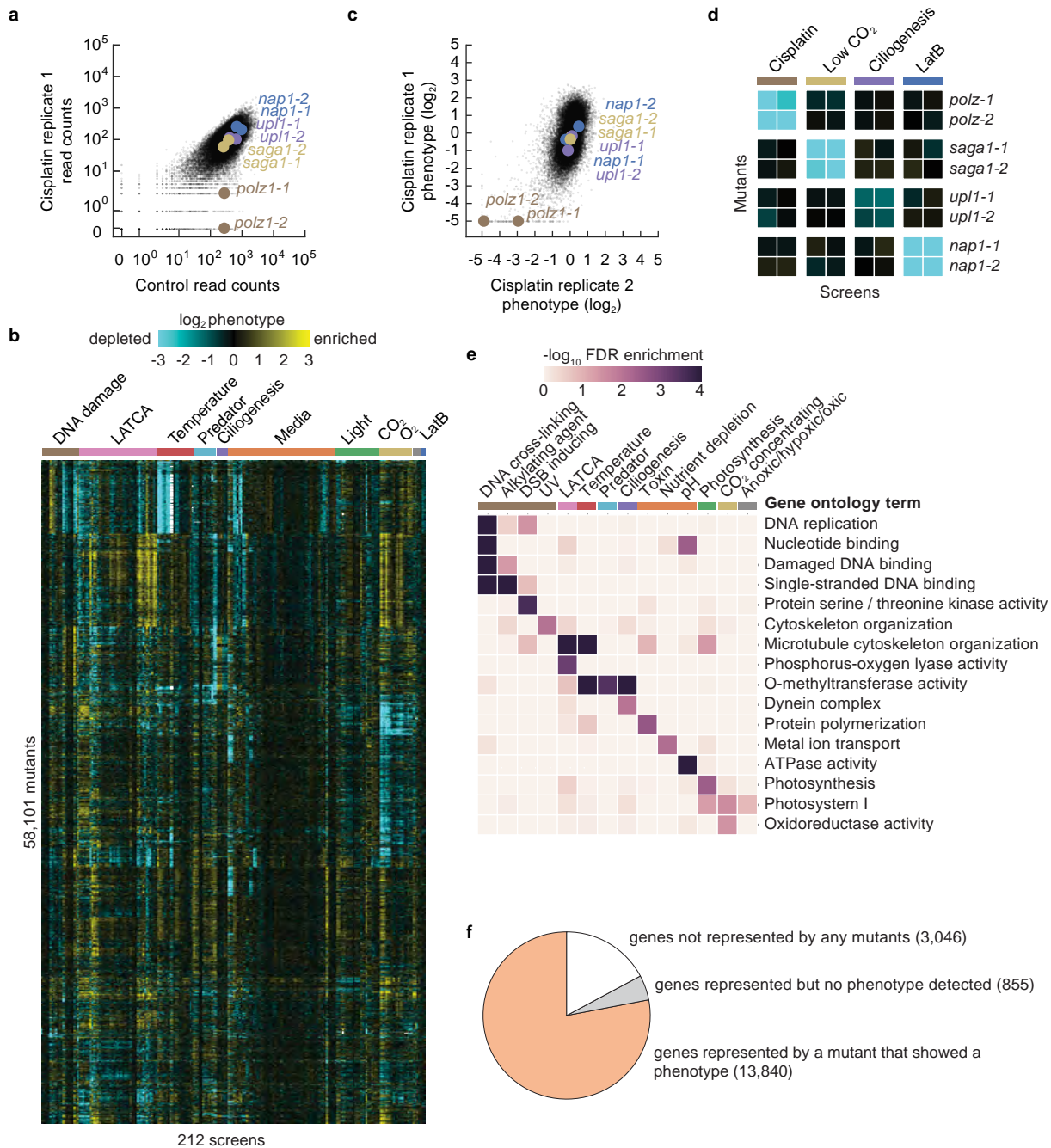
384 Figures and Legends



387 **Figure 1. We developed a platform for genotype-phenotype discovery in a unicellular**
388 **photosynthetic eukaryote.**

- 389 **a.** The *Chlamydomonas* mutant library was pooled and used to prepare a homogenous liquid
390 starting culture of 58,101 mutants.
- 391 **b.** Aliquots of the starting culture were used to inoculate pooled growth experiments to assess
392 the fitness of each mutant under a variety of environmental and chemical stress treatments.
- 393 **c.** The relative abundance of each mutant was quantified via PCR-based amplification of
394 individual mutant barcodes and subsequent Illumina sequencing.
- 395 **d.** Mutants negatively affected by the treatment have a lower barcode read count compared to
396 the control.
- 397 **e.** Many genes were represented by multiple mutants, which allowed the identification of
398 high-confidence gene phenotypes. We then clustered genes based on their phenotypic
399 profile to place genes into pathways and predict the functions of previously uncharacterized
400 genes.
- 401 **f.** The data predict gene function in *Chlamydomonas* and land plants.

402



403

404 **Figure 2. We determined the fitness of 58,101 Chlamydomonas mutants under 121 growth**
 405 **conditions.**

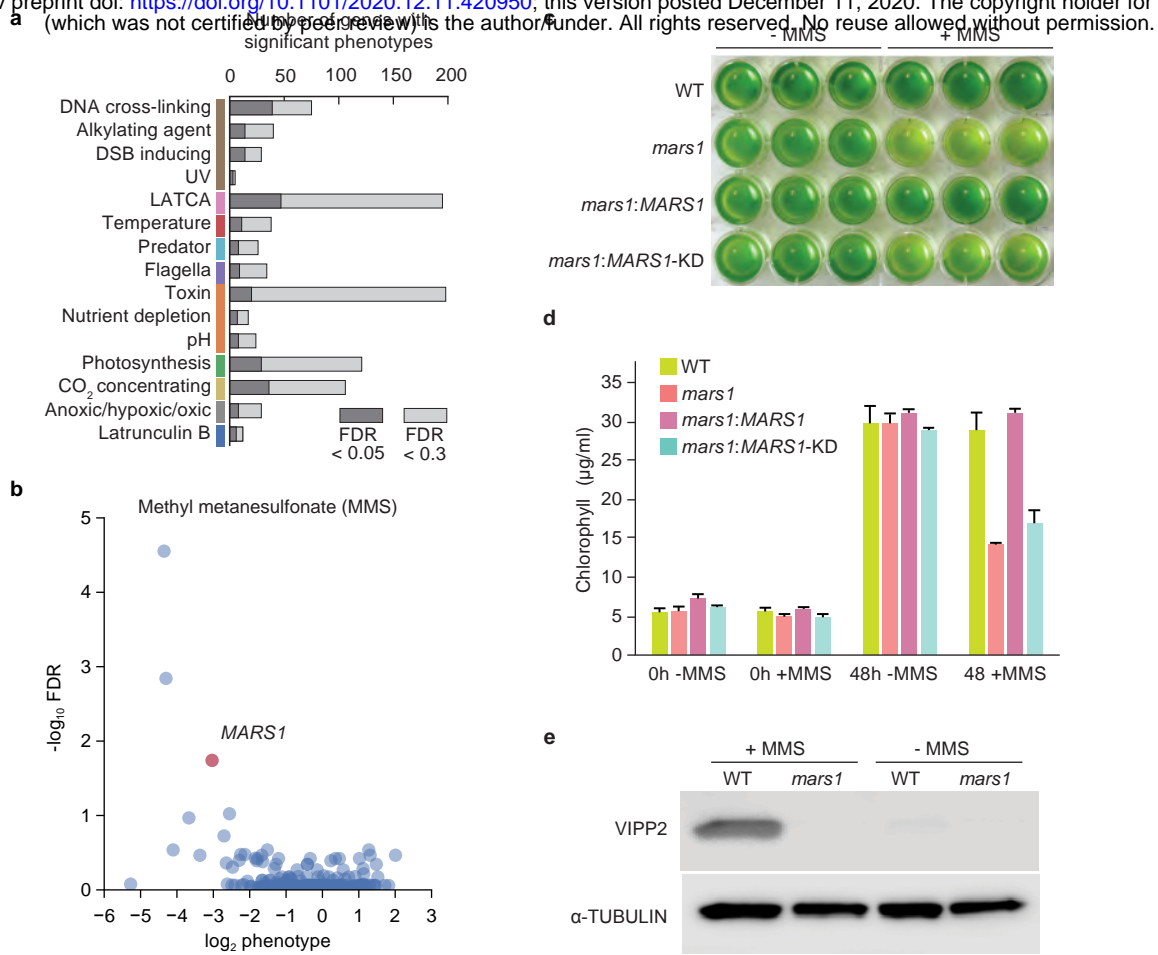
406 **a.** The phenotype of each mutant was determined by comparing its molecular barcode read
 407 count under a treatment and control condition. As an example, results from a screen using
 408 the drug cisplatin are shown.

409 **b.** The typical reproducibility is illustrated with two replicate cisplatin screens.

410 **c.** A hierarchically clustered heatmap shows the phenotype [\log_2 (treatment reads/control
 411 reads)] of mutants across 212 screens representing 121 growth conditions.

412 **d.** Mutants show screen-specific phenotypes.

- 413 **e.** Gene Ontology term analysis reveals enrichment of biological functions associated with
414 specific screens.
- 415 **f.** Most genes are represented by at least one mutant that shows a phenotype in at least one
416 treatment condition.



417

418 **Figure 3. Multiple alleles provide high confidence and reveal novel phenotypes.**

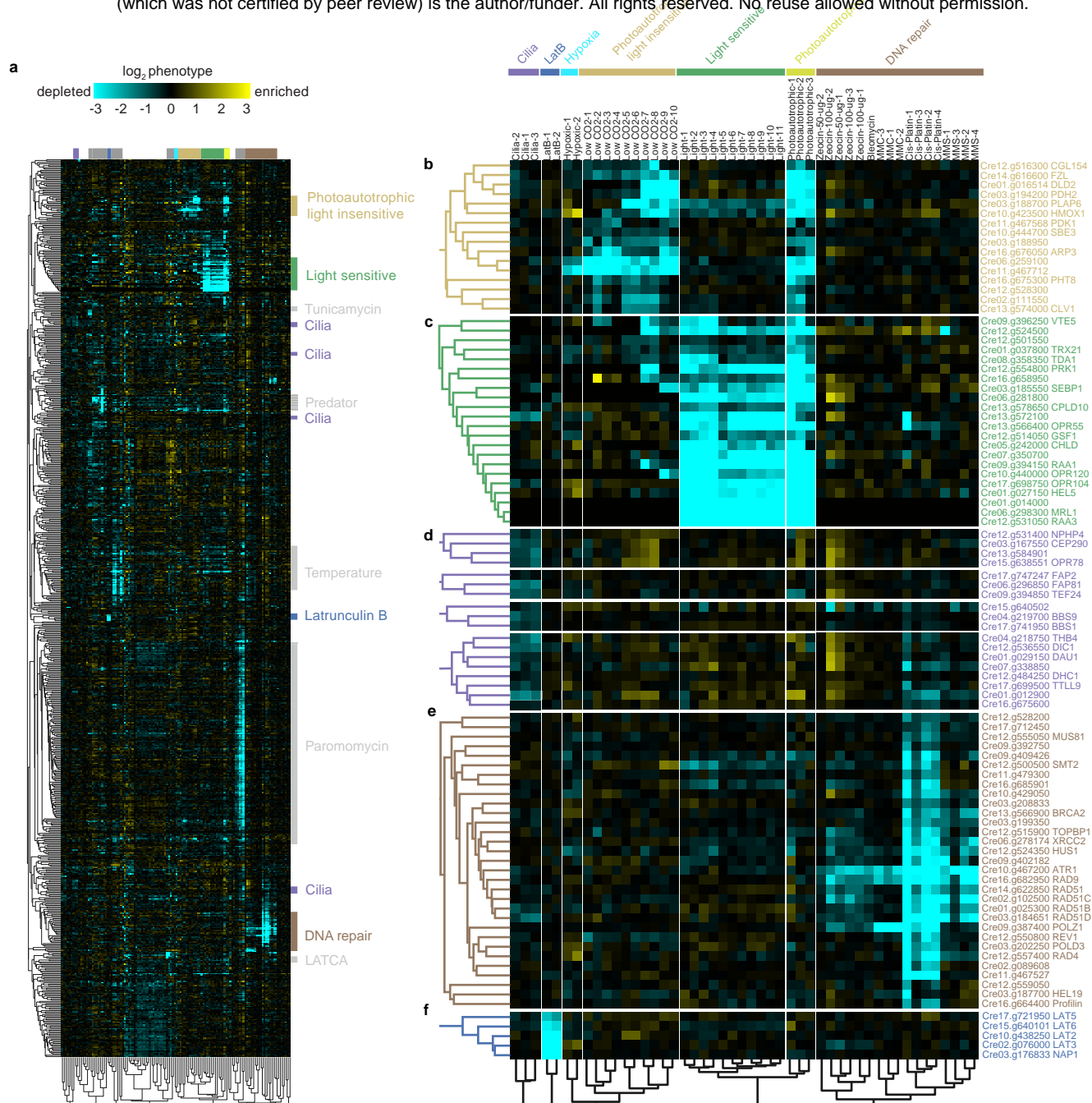
419 **a.** The number of genes with significant phenotypes in each class of screen is shown for two
420 false discovery rate (FDR) thresholds.

421 **b.** FDR is plotted against \log_2 median phenotype for all genes in the methyl methanesulfonate
422 (MMS) screen.

423 **c.** Growth assay of wild-type (WT), *mars1*, *mars1:MARS1*, and *mars1:MARS1 KD*
424 cells after 48 h in the presence or absence of MMS. Three biological replicates were used
425 for each strain. For more details, see materials and methods.

426 **d.** Average chlorophyll concentrations of the liquid cultures shown in Figure 3c.

427 **e.** Immunoblot analysis of VESICLE-INDUCING PROTEIN IN PLASTIDS (VIPP2), a
428 downstream target of MARS1, in WT and *mars1* cells in the presence or absence of MMS.

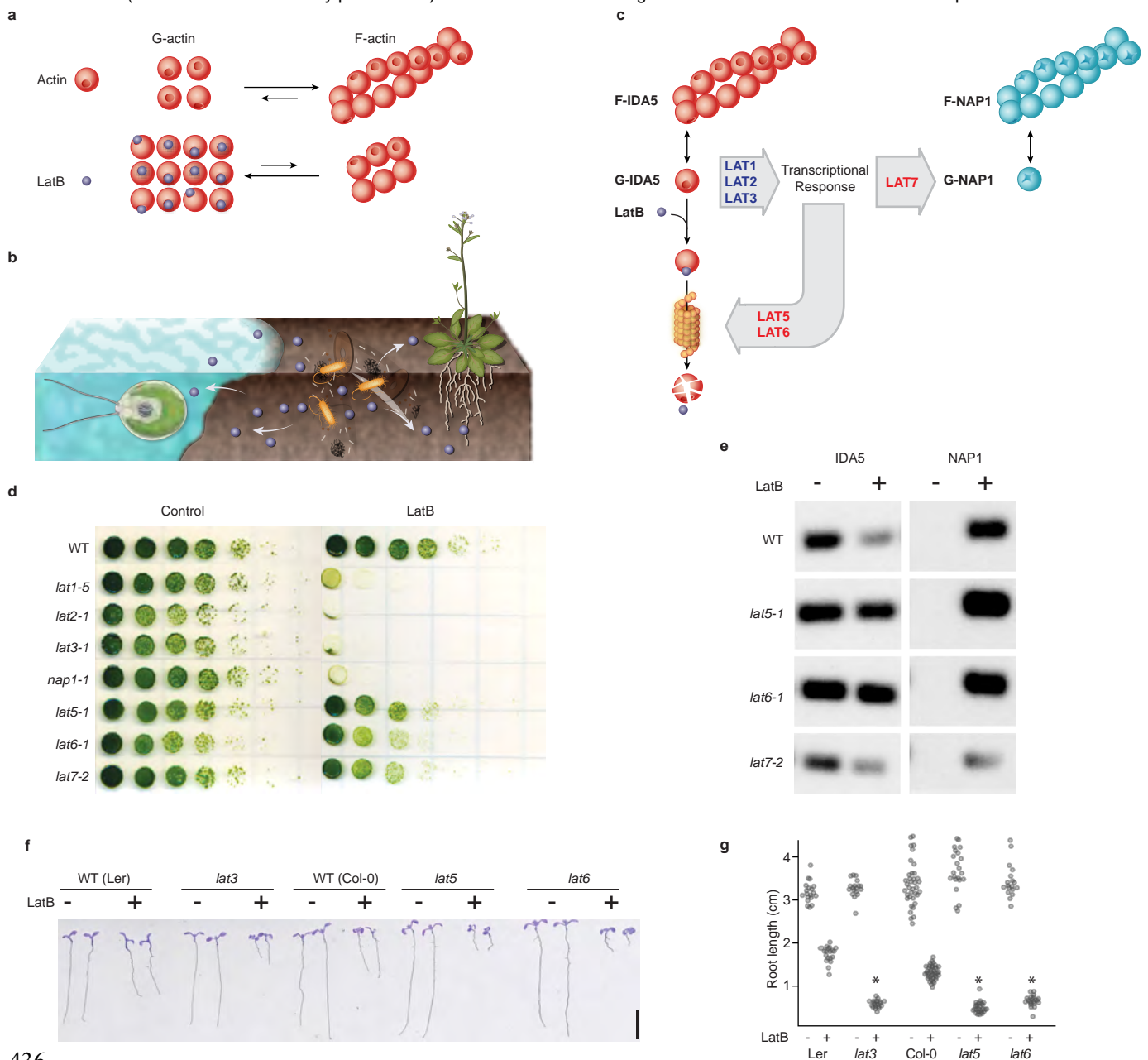


429

430 **Figure 4. Similarity of mutant phenotypes places genes into pathways and reveals novel**
 431 **players.**

432 a. 684 genes were clustered based on the similarity of their phenotypes across 120 screens.

433 b-f. Examples of how sub-clusters enriched in specific pathways predict novel genes in these
 434 pathways: b, non-photoautotrophic light-insensitive; c, non-photoautotrophic light-sensitive;
 435 d, cilia; e, DNA damage-sensitive; f, Latrunculin B-sensitive.



436

437 **Figure 5: The approach revealed novel conserved components of a defense mechanism**
 438 **against cytoskeleton inhibitors.**

439 **a.** Latrunculin B (LatB) interferes with actin polymerization.

440 **b.** Soil microorganisms deploy actin inhibitors for a competitive advantage in their
 441 environment.

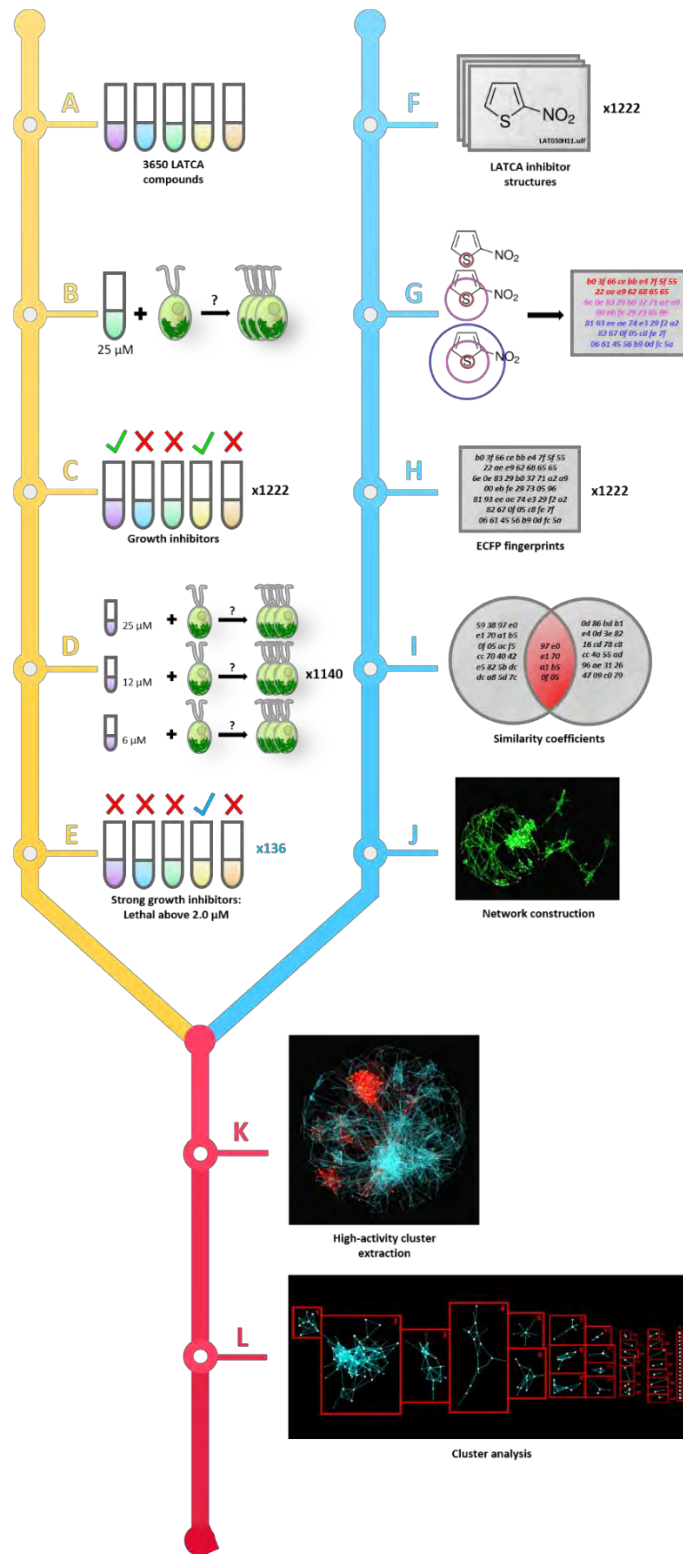
442 **c.** Chlamydomonas responds to actin inhibition by degrading its conventional actin IDA5 and
 443 upregulating an alternative actin, NAP1.

444 **d.** Growth of new *lat* mutants identified in this study (*lat5-1*, *lat6-1*, and *lat7-2*) was compared
 445 with previously isolated *lat1-5*, *lat2-1*, *lat3-1*, and *nap1-1* mutants⁶⁸ in the absence
 446 (control) and presence (LatB) of 3 μ M LatB.

- 447 **e.** Immunoblot of conventional (IDA5) and alternative (NAP1) actins shows that *lat5-1* and
448 *lat6-1* are deficient in actin degradation, while *lat7-2* lacks proper induction of the non-
449 canonical actin (NAP1) when exposed to an actin inhibitor.
- 450 **f.** The F-actin homeostasis pathway is conserved between green algae and plants. Mutants in
451 Arabidopsis genes homologous to Chlamydomonas *lat3*, *lat5*, and *lat6* show sensitivity to
452 LatB as decreased root length.
- 453 **g.** Quantification of root length in Arabidopsis mutants. Asterisks mark significant changes
454 based on two-way ANOVA, $p < 0.05$.

455 **Extended Data Figures and Tables**

456



457

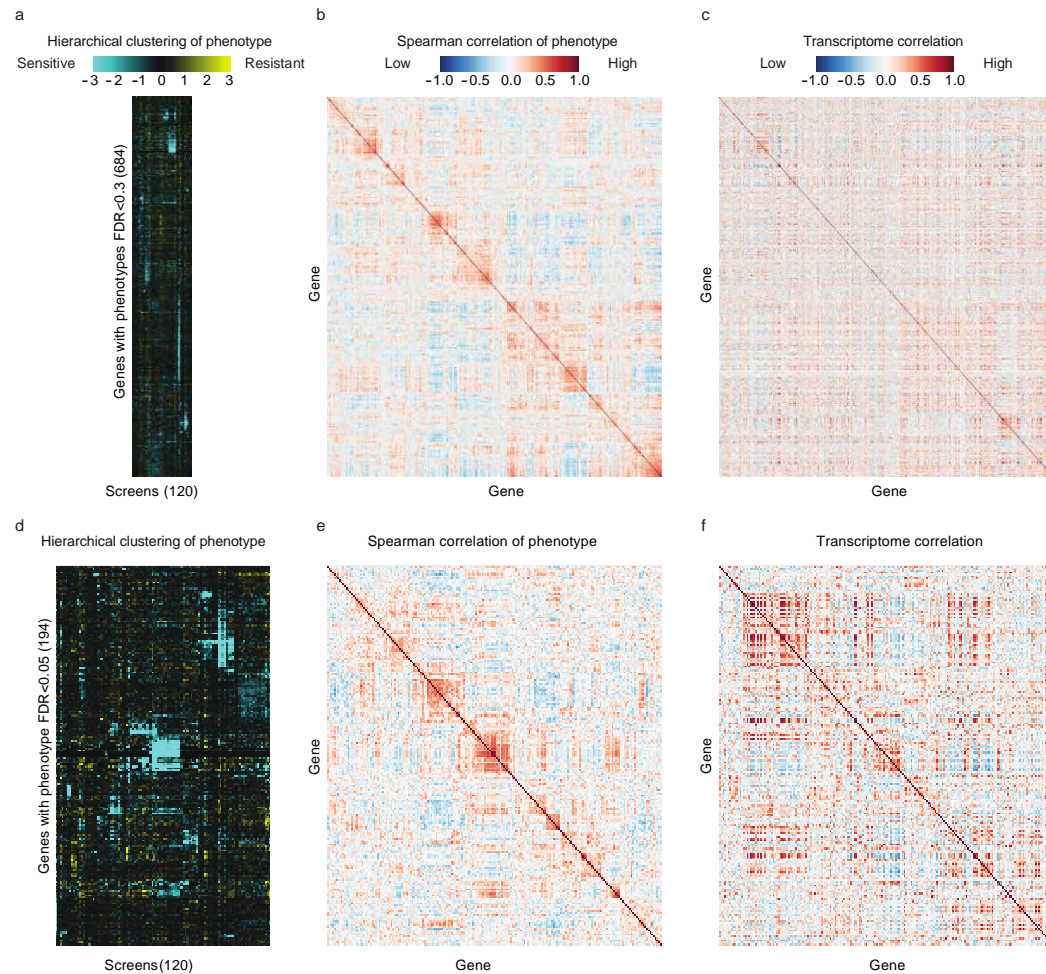
458 **Extended Data Figure 1. A screen of the chemical library “LATCA” identified 1,222**
459 **inhibitors of Chlamydomonas growth, 136 of which are active at 2 μ M or less.** Phase 1 of the
460 LATCA screen is depicted in A-E: The growth rate of wild-type Chlamydomonas (cMJ030) was
461 evaluated in TAP and TP in the presence of 3,650 LATCA compounds. 1,222 out of the 3,650
462 LATCA compounds reduced growth by 90% or more at 25 μ M (A–C). Dose-response experiments
463 were performed in TAP media with 1,140 out of the 1,222 highly active compounds that reduced
464 growth at 2 μ M or less (D,E). Phase 2 of the LATCA screen is depicted in F–J: Structural data
465 files (SDFs) were acquired for all LATCA inhibitors (F) and converted into numerical fingerprints
466 (extended-connectivity fingerprints; ECFPs) (G, H). ECFPs were then used to compute the
467 structural similarity of pairs of compounds using Tanimoto coefficients (I). The set of Tanimoto
468 coefficients between all pairs of inhibitors was condensed into a usable network (J). Phase 3 of the
469 LATCA screen is depicted in K and L: Data from A–E was used to further reduce the similarity
470 network from J to 28 clusters of structures exhibiting high levels of growth inhibition along with
471 a group of singleton structures (*) that did not cluster. Table S3 summarizes data A–E and shows
472 cluster annotations from L; see also Extended Data File 1 for all chemical structures from L.



473

474 **Extended Data Figure 2. Full GO term enrichments.** Gene Ontology term analysis reveals

475 enrichment of biological functions observed for specific screens. GO; FDR<0.05.



476

477 **Extended Data Figure 3. Comparison of phenotypic and transcriptomic correlations**

478 **a.** 684 genes were clustered based on the similarity of their phenotypes across 120 screens.

479 **b.** Spearman correlation matrix of phenotypes (FDR <0.3).

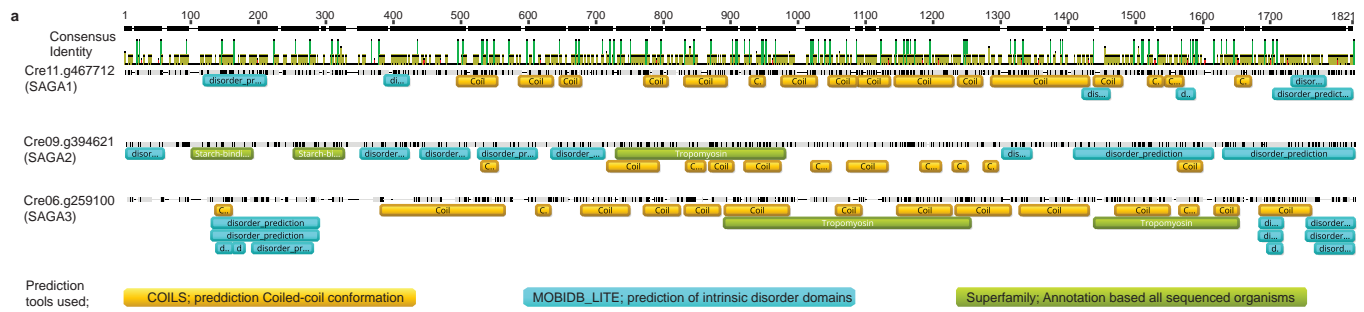
480 **c.** Transcriptome correlation of gene with phenotype (FDR <0.3).

481 **d.** 194 genes were clustered based on the similarity of their phenotype across 120 screens.

482 **e.** Spearman correlation matrix of phenotypes (FDR <0.05).

483 **f.** Transcriptome correlation of gene with phenotype (FDR <0.05).

484 Data can be found in Table S8.



b

Percentage of similarity based BLOSUM90 threshold=1

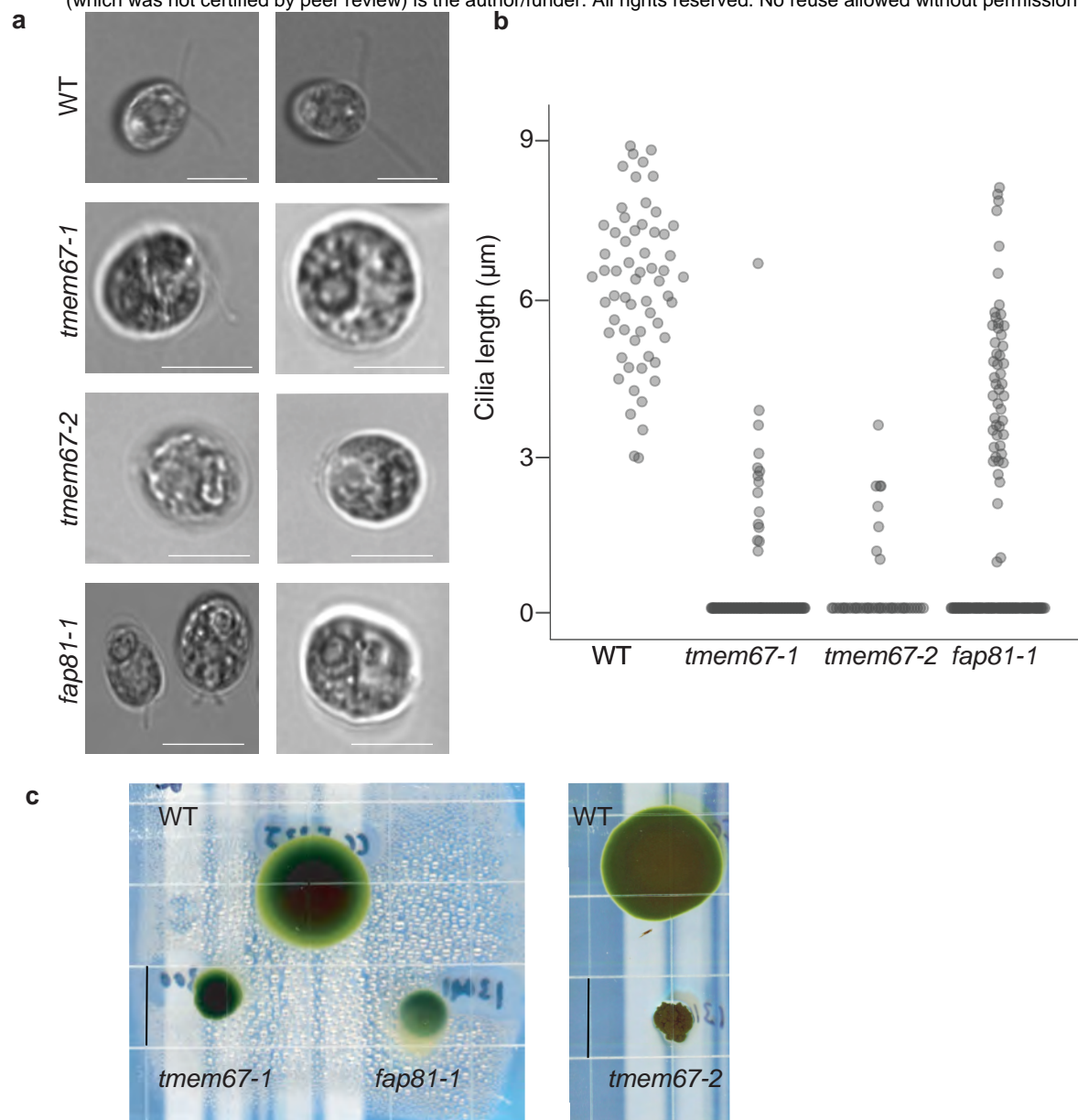
Gene	Cre11.g467712	Cre09.g394621	Cre06.g259100
Cre11.g467712 (SAGA1)		31.5	30.2
Cre09.g394621 (SAGA2)	31.5		24.7
Cre06.g259100 (SAGA3)	30.2	24.7	

485

486 **Extended Data Figure 4. SAGA protein alignments.**

487 **a.** Alignments of SAGA1, SAGA2, and SAGA3. Domain annotation was based on three
 488 different tools under the *Geneious* visualization platform.

489 **b.** BLOSUM90 alignments between SAGA proteins.



490

491 **Extended Data Figure 5. Validation of cilia mutant phenotypes.**

492 **a.** Bright-field microscopy microscope images of cilia mutants show defects in ciliary length.

493 Scale bar: 10 μ m.

494 **b.** Quantification of cilia length.

495 **c.** Swimming behavior of mutants, as determined by growth on TAP medium solidified with

496 0.15% agar. Scale bar: 5cm.

497 **LIST OF SUPPLEMENTARY MATERIALS**

498 Supplementary materials can be downloaded from the Chlamylibrary website:

499 <https://www.chlamylibrary.org/download>

500

501 Table S1 | Source material used for screens

502 Table S2 | List of screens

503 Table S3 | Initial LATCA screen and validation; cluster groups

504 Table S4 | Raw mutant phenotypes across all conditions

505 Table S5 | FDRs for GO term enrichment

506 Table S6 | FDRs for all genes by all screens

507 Table S7 | High-confidence gene-phenotype relationships

508 Table S8 | Phenotypic and transcriptomic correlations of genes with high-confidence phenotypes

509 Table S9 | Cluster annotations with yeast, mouse, and Arabidopsis orthologs

510 Table S10 | Primers used in this study

511 Table S11 | Raw and normalized read counts

512 Table S12 | List of samples that were averaged

513 Table S13 | Chlamydomonas and Arabidopsis strains used in this study

514 Extended Data File 1 | LATCA compound structures

515 Extended Data File 2 | Java TreeView files of FDR less than 0.3 gene clusters

516

517 **METHODS**

518 **Library maintenance**

519 The *Chlamydomonas* mutant collection¹² was maintained by robotically passaging 384-
520 colony arrays to fresh medium using a Singer RoToR robot (Singer Instruments, 704 Somerset,
521 UK). The mutant collection was grown on 1.5% agar Tris-Acetate-Phosphate (TAP) medium with
522 modified trace elements⁷¹ in complete darkness at room temperature. The routine passaging
523 interval of four weeks for library maintenance was shortened to two weeks during the time period
524 of pooled screens to increase cell viability.

525

526 **Screening of the Library of AcTive Compounds in Arabidopsis (LATCA) to identify** 527 ***Chlamydomonas* growth inhibitors**

528 The Library of AcTive Compounds in Arabidopsis (LATCA)¹³ was used to identify
529 molecules capable of inhibiting growth in wild-type *Chlamydomonas* (cMJ030). We found that
530 1,222 of these 3,650 LATCA compounds reduce growth by 90% at 25 μ M (Table S3). Due to
531 resource limitations, we could not perform competitive growth experiments with all 1,222 active
532 chemicals. Hence, we further selected the most active compounds and analyzed their structural
533 similarity to identify the most diverse set of compounds for the final screen. We performed dose-
534 response experiments with 1,140 compounds, validated activity for 954 compounds, and identified
535 136 chemicals that reduce growth at 2 μ M or less (Table S3). We then used the extended-
536 connectivity fingerprint (ECFP) algorithm⁷² to convert all LATCA compound structures into
537 numerical fingerprints. ECFPs were then used to compute structural similarity of pairs of
538 compounds on a scale of 0 to 1 using Tanimoto coefficients⁷³. The set of Tanimoto coefficients
539 between all pairs of inhibitors was condensed into a usable network and visualized using

540 Cytoscape⁷⁴. We then used the strongest inhibitors to further reduce the similarity network to 28
541 clusters of structures exhibiting high levels of biological activity and selected 52 of these chemicals
542 for subsequent treatment of the *Chlamydomonas* mutant library (Extended Data Fig. 1, Table S3,
543 and Extended Data File 1).

544

545 **Library pooling and competitive growth experiments**

546 The first two rounds of mutant library screening (R1, R2) were performed with the entire
547 mutant collection (550 384-mutant array plates) in 20-liter carboys (Table S1 and Table S2).
548 Mutants were pooled from five days old 384-colony array plates into liquid TAP medium at room
549 temperature and low light. In R1, we pooled ten copies of eight plates (#668 to #670) in the
550 collection to test how quantitatively we can track the relative abundance of mutants in the starting
551 population. In R2, we pooled one set of the mutant collection (plates #597 to #670) from 384-
552 colony array plates and another set from 1,536-colony array plates (#101 to #596) to test the
553 performance of denser colony arrays for pooled screens.

554 Subsequent rounds of mutant library screening (R3-R6) were performed on the re-arrayed
555 library (245 384-mutant array plates) in 2-liter bottles. Mutants were pooled from five days old
556 1,536-colony array plates. Condensing the library from 384 to 1,536-colony array plates helped to
557 both homogenize colony growth and reduce the laborious pooling procedure.

558 We produced subpools each containing cells from eight 384 or 1,535-colony array plates
559 by using sterile glass spreaders to pool cells the plates into 50 ml conical tubes containing 40 ml
560 of TAP medium. These subpools were mixed by pipetting to break cell clumps using a 10 ml
561 serological pipette with a P200 tip attached to it. Then, all subpools were combined into the final
562 mutant collection pool by pipetting the subpools through a 100 μ m cell strainer (VWR 10054-

563 458). The final pool was mixed using a magnetic stir bar, and the cell density was measured
564 (Countess, Invitrogen) and adjusted to 1×10^5 cells ml^{-1} . For experiments not performed in TAP
565 medium, cells were washed twice with the actual medium used for pooled screens after pelleting
566 ($1000 \times g$, 5 min, room temperature).

567 Aliquots of 2×10^8 cells were pelleted ($1000 \times g$, 5 min, room temperature) by centrifugation
568 and frozen to determine the relative abundance of each mutant in the starting population. These
569 samples are denoted as “Initial”.

570 Cultures were inoculated with 2×10^4 cells ml^{-1} in transparent 20-liter carboy tanks (R1 and
571 R2) or standard 2-liter bottles (R3 - R6) using aliquots of the final mutant pool. Cultures were
572 grown under a broad variety of conditions (Table S2). Unless otherwise indicated, cells were
573 grown in Tris-Acetate-Phosphate (TAP) medium with modified trace elements at pH 7.5 under
574 constant light ($100 \mu\text{mol photons m}^{-2} \text{s}^{-1}$) at 22°C , aerated with air and mixed using a conventional
575 magnetic stirrer at 200 rpm. The cell density of competitive growth experiments was tracked and
576 aliquots of 2×10^8 cells were pelleted by centrifugation after seven doublings, when the culture
577 reached approximately 2×10^6 cells ml^{-1} . Cell pellets were frozen for subsequent DNA extraction
578 and barcode quantification.

579

580 **DNA extraction**

581 Total genomic DNA was extracted from frozen cell pellets representing 2×10^8 cells of each
582 sample (initial, control, and treatment).

583 First, frozen pellets were thawed at room temperature and resuspended in 1.6 ml 0.5x SDS-
584 EB (1% SDS, 200 mM NaCl, 20 mM EDTA, and 50 mM Tris-HCl, pH 8.0).

585 Second, 2 ml of phenol:chloroform:isoamyl alcohol (25:24:1) was added to each sample
586 and mixed by vortexing. This solution was then transferred into 15 ml Qiagen MaXtract High
587 Density tubes (Cat No./ID: 129065) and centrifuged at 3,500 rpm for 5 minutes. Subsequently, the
588 aqueous phase was transferred to a new 15 ml conical tube, 6.4 μ l RNase A was added and the
589 solution was incubated at 37 °C for 30 minutes. The phenol/chloroform: isoamyl alcohol extraction
590 was then repeated, and the aqueous phase was transferred into a new 15 ml Qiagen MaXtract High
591 Density tube before adding 2 ml chloroform: isoamyl alcohol. This solution was mixed by
592 vortexing and centrifuged at 3,500 rpm for 5 minutes then, 400 μ l aliquots of the aqueous phase
593 were transferred to 1.5 ml reaction tubes for DNA precipitation.

594 Third, 1 ml of ice-cold 100% ethanol was added to the solution to precipitate DNA. The
595 tubes were gently mixed and incubated at -20 °C overnight. The DNA was pelleted at 13,200 rpm
596 and 4 °C. The supernatant was discarded and the pellet washed in 1 ml 70% ethanol. The
597 supernatant was discarded again and the pellet was air-dried before resuspension in 50 μ l water.
598 Subsequently, the elution fractions of each sample were pooled and the DNA concentration was
599 measured using a Qubit fluorometer (Invitrogen).

600

601 **Internal barcode amplification and Illumina library preparation**

602 Internal barcodes were amplified using Phusion Hot Start II (HSII) DNA Polymerase
603 (Thermo Fisher, F549L). Sequence information for all primers used in this study is summarized in
604 Table S10.

605 The 50 μ l PCR mixture for 5' barcode amplification contained: 125 ng genomic DNA, 10
606 μ l GC buffer, 5 μ l DMSO, 1 μ l dNTPs at 10 mM, 1 μ l MgCl₂ at 50 mM, 2.5 μ l of each primer at
607 10 μ M, and 1 μ l Phusion HSII polymerase. Eight tubes of the PCR mixture were processed per

608 sample and incubated at 98 °C for three minutes, followed by ten three-step cycles (98 °C for 10
609 s, 58 °C for 25 s and 72 °C for 15 s), and then eleven two-step cycles (98 °C for 10 s, 72 °C for 40
610 s).

611 The 50 µl PCR mixture for 3' barcode amplification contained: 125 ng genomic DNA, 10
612 µl GC buffer, 5 µl DMSO, 1 µl dNTPs at 10 mM, 2 µl MgCl₂ at 50 mM, 2.5 µl of each primer at
613 10 µM, and 1 µl Phusion HSII polymerase. Eight tubes of the PCR mixture were processed per
614 sample and incubated at 98 °C for three minutes, followed by ten three-step cycles (98 °C for 10
615 s, 63 °C for 25 s and 72 °C for 15 s), and then eleven two-step cycles (98 °C for 10 s, 72 °C for 40
616 s).

617 The PCR products of each sample were pooled for further processing. First, successful
618 PCR was confirmed on a TBE 8% agarose gel in 1 x Tris Borate EDTA before concentrating the
619 PCR products on a Qiagen MinElute column and measuring the DNA concentration on a Qubit
620 fluorometer. Second, 200-250 ng of up to 16 3' or 5' PCR products were combined into an Illumina
621 HiSeq2000 library. Third, the internal barcode bands of the Illumina HiSeq2000 libraries were gel-
622 purified and subjected to quality control on an Agilent Bioanalyzer. In addition, DNA
623 concentration was determined on a Qubit fluorometer. Fourth, HiSeq2000 libraries were
624 sequenced at the Genome Sequencing Service Center at Stanford University (3155 Porter Dr., Palo
625 Alto, CA 94304).

626

627 **Data analysis**

628 Initial reads were trimmed using cutadapt version 1.7.1⁷⁵ using the command "cutadapt -a
629 <seq> -e 0.1 -m 21 -M 23 input_file.gz -o output_file.fastq", where <seq> is
630 GGCAAGCTAGAGA for 5' data and TAGCGCGGGGCGT for 3' data. Barcodes were counted

631 by collapsing identical sequences using “fastx_collapser” (http://hannonlab.cshl.edu/fastx_toolkit)
632 and denoted as “_read_count”. Barcode read counts for each dataset were normalized to a total of
633 100 million and denoted as “_normalized_reads” (Table S11). Replicate control treatments
634 performed in the same screening round were averaged by taking the mean of the normalized read
635 counts to generate the average normalized read count and by summing the read counts to generate
636 the average read count. Control treatments that were averaged are denoted with “average” and can
637 be found in Table S12. Mutants in the library contain on average 1.2 insertions¹², each of which
638 may contain a 5’ barcode, a 3’ barcode, both barcodes, or potentially more than two barcodes if
639 multiple cassettes were inserted at the loci. To represent a given insertion within a mutant, we
640 selected a single barcode to represent it. All barcodes associated with the same gene and
641 deconvoluted to the same library well and plate position were assumed to be from the same
642 insertion and were then compared to identify the barcode with the highest read counts in the initial
643 samples (R2-R6) to serve as the representative barcode.

644 To identify mutants with growth defects or enhancements due to a specific treatment, we
645 compared the abundance of each mutant after growth under the treatment condition to its
646 abundance after growth under a control condition. We called this comparison a “screen”, and the
647 ratio of these abundances the “mutant phenotype”. In order for a phenotype to be calculated, we
648 required the control treatment to have a read count above 50.

649 To identify high-confidence gene-phenotype relationships we developed a statistical
650 framework that leverages multiple independent mutant alleles. For each gene, we generated a
651 contingency table of the phenotypes, P , by counting the number of alleles that met the following
652 thresholds: [$P < 0.0625$, $0.0625 \leq P < 0.125$, $0.125 \leq P < 0.25$, $0.25 \leq P < 0.5$, $0.5 \leq P < 2.0$, $2.0 \leq$
653 $P < 4.0$, $4.0 \leq P < 8.0$, $8.0 \leq P < 16.0$]. Only alleles that were confidence level 4 or less, had an

654 insertion in CDS/intron/5'UTR feature, and had greater than 50 reads in the control condition were
655 included in the analysis. A p-value was generated for each gene by using Fisher's exact test to
656 compare a gene's phenotype contingency table to a phenotype contingency table for all insertions
657 in the screen. A false discovery rate was performed on the p-values of genes with more than 2
658 alleles using the Benjamini-Hochberg method⁷⁶. To determine a representative phenotype for a
659 gene, the median phenotype for all alleles of that gene that were included in the Fisher's exact test
660 was used. For some analysis these gene phenotypes were normalized by setting the median value
661 of all gene phenotypes in a screen to zero. Clustering was performed with Python packages SciPy
662 and Seaborn. Data in Fig. 4a was clustered using the 'correlation' metric and 'average' method for
663 the linkage algorithm. Spearman and Pearson correlations were calculated in Pandas.
664 Transcriptome correlation data was collected, curated, and analyzed in the Merchant laboratory.
665 Data was plotted and visualized with the Python packages Matplotlib and Seaborn.

666 To determine if biological functions were associated with specific screens we performed a
667 Gene Ontology (GO) term enrichment analysis. Using the same approach as with genes, we
668 generated contingency tables of mutant phenotypes for each GO term. If a mutant's insertion is
669 within a gene that had multiple GO term annotations, the mutant's phenotype data was added to
670 each GO term's contingency table. A p-value was generated for each GO term by using Fisher's
671 exact test to compare a GO term's phenotype contingency table to a phenotype contingency table
672 for all GO terms in the screen. A false discovery rate was performed on the p-values using the
673 Benjamini-Hochberg method⁷⁶. Clustering were performed in the

674 All analysis was performed using JGI Phytozome release v5.0 of the *Chlamydomonas*
675 assembly and v5.6 of the *Chlamydomonas* annotation⁷⁷.

676

677 **Immunoblot materials IDA5, NAP1**

678 Cells were collected by centrifugation, frozen in liquid nitrogen, and subsequently
679 resuspended in 100 μ l of ice-cold PNE buffer (10 mM phosphate pH 7.0, 150 mM NaCl₂, 2 mM
680 EDTA) supplemented with a complete protease-inhibitor cocktail (Roche; 11697498001) and
681 disrupted by vortexing with acid-washed glass beads. In some experiments using anti-actin
682 antibodies, these samples were mixed directly with SDS-PAGE sample buffer, boiled for 3 min,
683 and cleared of debris by centrifugation at 12,000 x g for 10 min at 4 °C before electrophoresis. In
684 all other experiments, 100 μ l of PNE buffer + 2% NP-40 were added to the samples after cell
685 disruption, and the samples were then incubated for 10 min on ice and cleared by centrifugation at
686 12,000 x g for 10 min at 4 °C before adding SDS-PAGE sample buffer. We did not observe any
687 difference in abundance or solubility of IDA5 or NAP1 between the two methods. SDS-PAGE
688 was performed using 11% Tris-glycine (for IDA5 and NAP1). Blots were stained using a mouse
689 monoclonal anti-actin antibody (clone C4, EMD Millipore, MAB1501), which recognizes IDA5
690 but not NAP1; a rabbit antiNAP1 antibody (generous gift from Ritsu Kamiya and Takako Kato-
691 Minoura), which recognizes NAP1 but not IDA5. HRP-conjugated antimouse-IgG (ICN
692 Pharmaceuticals; 55564) or anti-rabbit-IgG (Southern Biotech; 4050-05) were used as secondary
693 antibodies. Figures showing blots are cropped to show only the molecular weight ranges of
694 interest: for IDA5 and NAP1, 37-50 kDa.

695

696 **MMS growth assays and VIPP2 immunoblot analysis**

697 The following strains were used¹⁷: WT = CC-4533; *mars1* = *mars1-3*; *mars1:MARS1-*
698 *D* = *mars1-3* transformed with the *MARS1-D* transgene containing a 3x-Flag epitope after
699 Met139; *mars1:MARS1-D KD* = *mars1-3* transformed with a catalytically-inactive *MARS1-*

700 *D* bearing the kinase active site D1871A mutation. Prior to starting liquid cultures in TAP media,
701 all strains were restreaked in fresh TAP plates and grown in similar light conditions (i.e., ~50–70
702 $\mu\text{mol photons m}^{-2} \text{ s}^{-1}$, ~22 °C) for about 5-6 days. Prior to starting the MMS treatment, all strains
703 were pre-conditioned in liquid cultures for about 3-4 days. Next, cell cultures were equally diluted
704 to ~5 $\mu\text{g chlorophyll ml}^{-1}$ and incubated in the presence or absence of MMS for 48 hours. A 1%
705 (vol/vol) MMS stock solution (Sigma Aldrich # 129925) was freshly prepared in ddH₂O at the
706 beginning of each experiment. This MMS stock solution was further diluted 200 times directly
707 into TAP media to a final concentration of 0.05% (vol/vol). All chlorophyll concentration
708 measurements were performed using a previously described methanol extraction method⁷⁸.

709 VIPP2 and alpha-TUBULIN immunoblot analyses were carried out as described¹⁷, using
710 denatured total protein samples prepared from liquid cultures incubated for 27 hours in the
711 presence or absence of 0.05% (vol/vol) MMS.

712

713 **Cilia and LatB-related Chlamydomonas experiments**

714 Mutants used in this study are listed in Table S13. Individual mutants were grown with
715 gentle agitation at 100 $\mu\text{mol photons m}^{-2} \text{ s}^{-1}$. Disruption of *LAT5*, *LAT6*, and *LAT7* genes
716 (Cre17.g721950, Cre15.g640101, and Cre11.g482750) in the original isolates of *lat5-1*, *lat6-1*,
717 *lat7-2* were confirmed by PCR. These mutants were then backcrossed with CC-124 or CC-125
718 three times, with perfect linkage of paromomycin resistance and LatB sensitivity in at least 10
719 tetrads confirmed after each round. The backcrossed strains and the previously established *lat1-5*,
720 *lat2-1*, *lat3-1*, and *nap1-1* mutants in the CC-124 background⁶⁸ were spotted on TAP agar
721 containing 0.1% DMSO with or without 3 μM LatB as 5x serial dilutions.

722 Cilia mutants were grown in liquid TAP medium until they reached exponential phase.
723 Cells were then mounted in u-Slide 8-well chambers (Ibidi, 80826) with 2% low melting point
724 agarose (Sigma, A9414). Cilia defects were scored using a Leica DMI8 inverted microscope. Cilia
725 length was measured using Fiji. Cilia swimming behavior was scored using TAP agar plates with
726 0.15% agar. Latrunculin B (Sigma, L5288) treatments were performed on TAP agar plates
727 supplemented with 3 μ M LatB and spotted in 10-fold serial dilutions.

728

729 **Arabidopsis experiments**

730 Mutants used in this study are listed in Table S13. Seeds were surface-sterilized in 20%
731 bleach for 5 min. Seeds were then rinsed with sterile water four times and stored at 4 °C for three
732 days in the dark. After stratification, seeds were sown into square 10 cm x 10 cm petri plates
733 containing full strength Murashige and Skoog (MS) medium (MSP01-50LT), 1% agar (Duchefa,
734 9002-18-0), 1% sucrose, 0.05% MES, and adjusted to pH 5.7 with 1 M KOH. Seedlings were
735 grown in the presence of LatB (Sigma, L5288) or mock control containing equivalent volume of
736 the LatB solvent, DMSO. Plates were imaged using a CanonScan 9000 flatbed scanner. Root
737 lengths were quantified using Fiji. Two-way ANOVA and data visualization were done using
738 Python.

739

740 References

- 741 1 Bassham, J. A. *et al.* The Path of Carbon in Photosynthesis. XXI. The Cyclic Regeneration of
742 Carbon Dioxide Acceptor1. *Journal of the American Chemical Society* **76**, 1760-1770,
743 doi:10.1021/ja01636a012 (1954).
- 744 2 Deisenhofer, J., Epp, O., Miki, K., Huber, R. & Michel, H. X-ray structure analysis of a
745 membrane protein complex. Electron density map at 3 Å resolution and a model of the
746 chromophores of the photosynthetic reaction center from *Rhodospseudomonas viridis*. *J Mol Biol*
747 **180**, 385-398, doi:10.1016/s0022-2836(84)80011-x (1984).
- 748 3 Levine, R. P. Genetic dissection of photosynthesis. *Science* **162**, 768-771,
749 doi:10.1126/science.162.3855.768 (1968).
- 750 4 Mayfield, S. P., Rahire, M., Frank, G., Zuber, H. & Rochaix, J. D. Expression of the nuclear gene
751 encoding oxygen-evolving enhancer protein 2 is required for high levels of photosynthetic
752 oxygen evolution in *Chlamydomonas reinhardtii*. *Proc Natl Acad Sci U S A* **84**, 749-753,
753 doi:10.1073/pnas.84.3.749 (1987).
- 754 5 Hillenmeyer, M. E. *et al.* The chemical genomic portrait of yeast: uncovering a phenotype for all
755 genes. *Science* **320**, 362-365, doi:10.1126/science.1150021 (2008).
- 756 6 Harris, E. H., Stern, D. B. & Witman, G. B. *The Chlamydomonas Sourcebook: Introduction to*
757 *Chlamydomonas and Its Laboratory Use*. (Elsevier Science, 2009).
- 758 7 Ostrowski, L. E., Dutcher, S. K. & Lo, C. W. Cilia and models for studying structure and
759 function. *Proc Am Thorac Soc* **8**, 423-429, doi:10.1513/pats.201103-027SD (2011).
- 760 8 Lefebvre, P. A. & Rosenbaum, J. L. Regulation of the synthesis and assembly of ciliary and
761 flagellar proteins during regeneration. *Annu Rev Cell Biol* **2**, 517-546,
762 doi:10.1146/annurev.cb.02.110186.002505 (1986).
- 763 9 Luck, D. J. Genetic and biochemical dissection of the eucaryotic flagellum. *J Cell Biol* **98**, 789-
764 794, doi:10.1083/jcb.98.3.789 (1984).
- 765 10 Park, R. V., Asbury, H. & Miller, S. M. Modification of a *Chlamydomonas reinhardtii*
766 CRISPR/Cas9 transformation protocol for use with widely available electroporation equipment.
767 *MethodsX* **7**, 100855, doi:10.1016/j.mex.2020.100855 (2020).
- 768 11 Greiner, A. *et al.* Targeting of Photoreceptor Genes in *Chlamydomonas reinhardtii* via Zinc-
769 Finger Nucleases and CRISPR/Cas9. *Plant Cell* **29**, 2498-2518, doi:10.1105/tpc.17.00659 (2017).
- 770 12 Li, X. *et al.* A genome-wide algal mutant library and functional screen identifies genes required
771 for eukaryotic photosynthesis. *Nat Genet* **51**, 627-635, doi:10.1038/s41588-019-0370-6 (2019).
- 772 13 Zhao, Y. *et al.* Chemical genetic interrogation of natural variation uncovers a molecule that is
773 glycoactivated. *Nat Chem Biol* **3**, 716-721, doi:10.1038/nchembio.2007.32 (2007).

- 774 14 Ashburner, M. *et al.* Gene ontology: tool for the unification of biology. The Gene Ontology
775 Consortium. *Nat Genet* **25**, 25-29, doi:10.1038/75556 (2000).
- 776 17 Perlaza, K. *et al.* The Mars1 kinase confers photoprotection through signaling in the chloroplast
777 unfolded protein response. *Elife* **8**, doi:10.7554/eLife.49577 (2019).
- 778 19 Hakem, R. DNA-damage repair; the good, the bad, and the ugly. *EMBO J* **27**, 589-605,
779 doi:10.1038/emboj.2008.15 (2008).
- 780 20 Vlcek, D., Sevcovicova, A., Sviezena, B., Galova, E. & Miadokova, E. *Chlamydomonas*
781 *reinhardtii*: a convenient model system for the study of DNA repair in photoautotrophic
782 eukaryotes. *Curr Genet* **53**, 1-22, doi:10.1007/s00294-007-0163-9 (2008).
- 783 21 Culligan, K., Tissier, A. & Britt, A. ATR regulates a G2-phase cell-cycle checkpoint in
784 *Arabidopsis thaliana*. *Plant Cell* **16**, 1091-1104, doi:10.1105/tpc.018903 (2004).
- 785 22 Heitzeberg, F. *et al.* The Rad17 homologue of *Arabidopsis* is involved in the regulation of DNA
786 damage repair and homologous recombination. *Plant J* **38**, 954-968, doi:10.1111/j.1365-
787 313X.2004.02097.x (2004).
- 788 23 Garcia, V., Salanoubat, M., Choisne, N. & Tissier, A. An ATM homologue from *Arabidopsis*
789 *thaliana*: complete genomic organisation and expression analysis. *Nucleic Acids Res* **28**, 1692-
790 1699, doi:10.1093/nar/28.8.1692 (2000).
- 791 24 Feng, W. *et al.* Genetic determinants of cellular addiction to DNA polymerase theta. *Nat*
792 *Commun* **10**, 4286, doi:10.1038/s41467-019-12234-1 (2019).
- 793 25 Plecenikova, A., Slaninova, M. & Riha, K. Characterization of DNA repair deficient strains of
794 *Chlamydomonas reinhardtii* generated by insertional mutagenesis. *PLoS One* **9**, e105482,
795 doi:10.1371/journal.pone.0105482 (2014).
- 796 26 Recker, J., Knoll, A. & Puchta, H. The *Arabidopsis thaliana* homolog of the helicase RTEL1
797 plays multiple roles in preserving genome stability. *Plant Cell* **26**, 4889-4902,
798 doi:10.1105/tpc.114.132472 (2014).
- 799 27 Knoll, A. *et al.* The Fanconi anemia ortholog FANCM ensures ordered homologous
800 recombination in both somatic and meiotic cells in *Arabidopsis*. *Plant Cell* **24**, 1448-1464,
801 doi:10.1105/tpc.112.096644 (2012).
- 802 28 Hartung, F., Suer, S., Bergmann, T. & Puchta, H. The role of AtMUS81 in DNA repair and its
803 genetic interaction with the helicase AtRecQ4A. *Nucleic Acids Res* **34**, 4438-4448,
804 doi:10.1093/nar/gkl576 (2006).
- 805 29 Perron, K., Goldschmidt-Clermont, M. & Rochaix, J. D. A factor related to pseudouridine
806 synthases is required for chloroplast group II intron trans-splicing in *Chlamydomonas reinhardtii*.
807 *EMBO J*. **18**, 6481-6490, doi:10.1093/emboj/18.22.6481 (1999).

- 808 30 Jacobs, J. *et al.* Identification of a chloroplast ribonucleoprotein complex containing trans-
809 splicing factors, intron RNA, and novel components. *Mol. Cell. Proteomics* **12**, 1912-1925,
810 doi:10.1074/mcp.M112.026583 (2013).
- 811 31 Marx, C., Wünsch, C. & Kück, U. The Octatricopeptide Repeat Protein Raa8 Is Required for
812 Chloroplast trans Splicing. *Eukaryot. Cell* **14**, 998-1005, doi:10.1128/EC.00096-15 (2015).
- 813 32 Schult, K. *et al.* The nuclear-encoded factor HCF173 is involved in the initiation of translation of
814 the psbA mRNA in *Arabidopsis thaliana*. *Plant Cell* **19**, 1329-1346, doi:10.1105/tpc.106.042895
815 (2007).
- 816 33 Brzezowski, P. *et al.* Mg chelatase in chlorophyll synthesis and retrograde signaling in
817 *Chlamydomonas reinhardtii*: CHLI2 cannot substitute for CHLI1. *J Exp Bot* **67**, 3925-3938,
818 doi:10.1093/jxb/erw004 (2016).
- 819 34 Eberhard, S. *et al.* Dual functions of the nucleus-encoded factor TDA1 in trapping and translation
820 activation of atpA transcripts in *Chlamydomonas reinhardtii* chloroplasts. *Plant J* **67**, 1055-1066,
821 doi:10.1111/j.1365-313X.2011.04657.x (2011).
- 822 35 Johnson, X. *et al.* MRL1, a conserved Pentatricopeptide repeat protein, is required for
823 stabilization of rbcL mRNA in *Chlamydomonas* and *Arabidopsis*. *Plant Cell* **22**, 234-248,
824 doi:10.1105/tpc.109.066266 (2010).
- 825 36 Liu, X. L., Yu, H. D., Guan, Y., Li, J. K. & Guo, F. Q. Carbonylation and loss-of-function
826 analyses of SBPase reveal its metabolic interface role in oxidative stress, carbon assimilation, and
827 multiple aspects of growth and development in *Arabidopsis*. *Mol Plant* **5**, 1082-1099,
828 doi:10.1093/mp/sss012 (2012).
- 829 37 Brandes, H. K., Larimer, F. W. & Hartman, F. C. The molecular pathway for the regulation of
830 phosphoribulokinase by thioredoxin f. *J Biol Chem* **271**, 3333-3335, doi:10.1074/jbc.271.7.3333
831 (1996).
- 832 38 Klein, R. R. & Houtz, R. L. Cloning and developmental expression of pea ribulose-1,5-
833 bisphosphate carboxylase/oxygenase large subunit N-methyltransferase. *Plant Mol Biol* **27**, 249-
834 261, doi:10.1007/BF00020181 (1995).
- 835 39 Wang, Y., Stessman, D. J. & Spalding, M. H. The CO₂ concentrating mechanism and
836 photosynthetic carbon assimilation in limiting CO₂ : how *Chlamydomonas* works against the
837 gradient. *Plant J.* **82**, 429-448, doi:10.1111/tpj.12829 (2015).
- 838 40 Wang, Y. & Spalding, M. H. Acclimation to Very Low CO₂: Contribution of Limiting CO₂
839 Inducible Proteins, LCIB and LCIA, to Inorganic Carbon Uptake in *Chlamydomonas reinhardtii*.
840 *Plant Physiol.* **166**, 2040-2050, doi:10.1104/pp.114.248294 (2014).

- 841 41 Moroney, J. V. *et al.* The carbonic anhydrase isoforms of *Chlamydomonas reinhardtii*:
842 intracellular location, expression, and physiological roles. *Photosynth. Res.* **109**, 133-149,
843 doi:10.1007/s11120-011-9635-3 (2011).
- 844 42 Wang, Y. & Spalding, M. H. An inorganic carbon transport system responsible for acclimation
845 specific to air levels of CO₂ in *Chlamydomonas reinhardtii*. *Proc Natl Acad Sci U S A* **103**,
846 10110-10115, doi:10.1073/pnas.0603402103 (2006).
- 847 43 Fukuzawa, H. *et al.* Ccm1, a regulatory gene controlling the induction of a carbon-concentrating
848 mechanism in *Chlamydomonas reinhardtii* by sensing CO₂ availability. *Proc. Natl. Acad. Sci. U.*
849 *S. A.* **98**, 5347-5352, doi:10.1073/pnas.081593498 (2001).
- 850 44 Xiang, Y., Zhang, J. & Weeks, D. P. The Cia5 gene controls formation of the carbon
851 concentrating mechanism in *Chlamydomonas reinhardtii*. *Proc Natl Acad Sci U S A* **98**, 5341-
852 5346, doi:10.1073/pnas.101534498 (2001).
- 853 45 Itakura, A. K. *et al.* A Rubisco-binding protein is required for normal pyrenoid number and starch
854 sheath morphology in *Chlamydomonas reinhardtii*. *Proc. Natl. Acad. Sci. U. S. A.* **116**, 18445-
855 18454, doi:10.1073/pnas.1904587116 (2019).
- 856 46 Meyer, M. T. *et al.* Assembly of the algal CO₂-fixing organelle, the pyrenoid, is guided by a
857 Rubisco-binding motif. *Science Advances* **6**, eabd2408, doi:10.1126/sciadv.abd2408 (2020).
- 858 47 Kobayashi, Y. *et al.* Eukaryotic Components Remodeled Chloroplast Nucleoid Organization
859 during the Green Plant Evolution. *Genome Biol Evol* **8**, 1-16, doi:10.1093/gbe/evv233 (2015).
- 860 48 Mackinder, L. C. M. *et al.* A Spatial Interactome Reveals the Protein Organization of the Algal
861 CO₂-Concentrating Mechanism. *Cell* **171**, 133-147.e114, doi:10.1016/j.cell.2017.08.044 (2017).
- 862 49 Toyokawa, C., Yamano, T. & Fukuzawa, H. Pyrenoid Starch Sheath Is Required for LCIB
863 Localization and the CO₂-Concentrating Mechanism in Green Algae. *Plant Physiol* **182**, 1883-
864 1893, doi:10.1104/pp.19.01587 (2020).
- 865 50 Findinier, J., Delevoye, C. & Cohen, M. M. The dynamin-like protein Fzl promotes thylakoid
866 fusion and resistance to light stress in *Chlamydomonas reinhardtii*. *PLoS Genet.* **15**, e1008047,
867 doi:10.1371/journal.pgen.1008047 (2019).
- 868 51 Mackinder, L. C. M. *et al.* A repeat protein links Rubisco to form the eukaryotic carbon-
869 concentrating organelle. *Proc. Natl. Acad. Sci. U. S. A.* **113**, 5958-5963,
870 doi:10.1073/pnas.1522866113 (2016).
- 871 52 Yamano, T. *et al.* Light and Low-CO₂-Dependent LCIB–LCIC Complex Localization in the
872 Chloroplast Supports the Carbon-Concentrating Mechanism in *Chlamydomonas reinhardtii*. *Plant*
873 *Cell Physiol.* **51**, 1453-1468, doi:10.1093/pcp/pcq105 (2010).

- 874 53 Turkina, M. V., Blanco-Rivero, A., Vainonen, J. P., Vener, A. V. & Villarejo, A. CO2 limitation
875 induces specific redox-dependent protein phosphorylation in *Chlamydomonas reinhardtii*.
876 *Proteomics* **6**, 2693-2704, doi:10.1002/pmic.200500461 (2006).
- 877 54 Zhan, Y. *et al.* Pyrenoid functions revealed by proteomics in *Chlamydomonas reinhardtii*. *PLoS*
878 *One* **13**, e0185039, doi:10.1371/journal.pone.0185039 (2018).
- 879 55 Pazour, G. J., Agrin, N., Leszyk, J. & Witman, G. B. Proteomic analysis of a eukaryotic cilium. *J.*
880 *Cell Biol.* **170**, 103-113, doi:10.1083/jcb.200504008 (2005).
- 881 56 Awata, J. *et al.* NPHP4 controls ciliary trafficking of membrane proteins and large soluble
882 proteins at the transition zone. *J. Cell Sci.* **127**, 4714-4727, doi:10.1242/jcs.155275 (2014).
- 883 57 Collin, G. B. *et al.* Meckelin is necessary for photoreceptor intraciliary transport and outer
884 segment morphogenesis. *Invest. Ophthalmol. Vis. Sci.* **53**, 967-974, doi:10.1167/iovs.11-8766
885 (2012).
- 886 58 Craige, B. *et al.* CEP290 tethers flagellar transition zone microtubules to the membrane and
887 regulates flagellar protein content. *J. Cell Biol.* **190**, 927-940, doi:10.1083/jcb.201006105 (2010).
- 888 59 Liu, P. & Lechtreck, K. F. The Bardet–Biedl syndrome protein complex is an adapter expanding
889 the cargo range of intraflagellar transport trains for ciliary export. *Proc. Natl. Acad. Sci. U. S. A.*
890 **115**, E934-E943, doi:10.1073/pnas.1713226115 (2018).
- 891 60 Mitchison, H. M. *et al.* Mutations in axonemal dynein assembly factor DNAAF3 cause primary
892 ciliary dyskinesia. *Nat. Genet.* **44**, 381-389, S381-382, doi:10.1038/ng.1106 (2012).
- 893 61 Hom, E. F. Y. *et al.* A unified taxonomy for ciliary dyneins. *Cytoskeleton* **68**, 555-565,
894 doi:10.1002/cm.20533 (2011).
- 895 62 Kamiya, R. Mutations at twelve independent loci result in absence of outer dynein arms in
896 *Chlamydomonas reinhardtii*. *J. Cell Biol.* **107**, 2253-2258, doi:10.1083/jcb.107.6.2253 (1988).
- 897 63 Myster, S. H., Knott, J. A., O'Toole, E. & Porter, M. E. The *Chlamydomonas* Dhc1 gene encodes
898 a dynein heavy chain subunit required for assembly of the II inner arm complex. *Mol. Biol. Cell*
899 **8**, 607-620, doi:10.1091/mbc.8.4.607 (1997).
- 900 64 Kubo, T., Yanagisawa, H.-A., Yagi, T., Hirono, M. & Kamiya, R. Tubulin Polyglutamylation
901 Regulates Axonemal Motility by Modulating Activities of Inner-Arm Dyneins. *Curr. Biol.* **20**,
902 441-445, doi:10.1016/j.cub.2009.12.058 (2010).
- 903 65 Verdier, P., Morthorst, S. K. & Pedersen, L. B. Targeting of ASH Domain-Containing Proteins to
904 the Centrosome. *Methods Mol. Biol.* **1454**, 15-33, doi:10.1007/978-1-4939-3789-9_2 (2016).
- 905 66 Morton, W. M., Ayscough, K. R. & McLaughlin, P. J. Latrunculin alters the actin-monomer
906 subunit interface to prevent polymerization. *Nat Cell Biol* **2**, 376-378, doi:10.1038/35014075
907 (2000).

- 908 67 Spector, I., Shochet, N. R., Kashman, Y. & Groweiss, A. Latrunculins: novel marine toxins that
909 disrupt microfilament organization in cultured cells. *Science* **219**, 493-495,
910 doi:10.1126/science.6681676 (1983).
- 911 68 Onishi, M., Pringle, J. R. & Cross, F. R. Evidence That an Unconventional Actin Can Provide
912 Essential F-Actin Function and That a Surveillance System Monitors F-Actin Integrity in
913 *Chlamydomonas*. *Genetics* **202**, 977-996, doi:10.1534/genetics.115.184663 (2016).
- 914 69 Onishi, M., Pecani, K., Jones, T. t., Pringle, J. R. & Cross, F. R. F-actin homeostasis through
915 transcriptional regulation and proteasome-mediated proteolysis. *Proc Natl Acad Sci U S A* **115**,
916 E6487-E6496, doi:10.1073/pnas.1721935115 (2018).
- 917 70 Feldman, R. M., Correll, C. C., Kaplan, K. B. & Deshaies, R. J. A complex of Cdc4p, Skp1p, and
918 Cdc53p/cullin catalyzes ubiquitination of the phosphorylated CDK inhibitor Sic1p. *Cell* **91**, 221-
919 230, doi:10.1016/s0092-8674(00)80404-3 (1997).
- 920 71 Kropat, J. *et al.* A revised mineral nutrient supplement increases biomass and growth rate in
921 *Chlamydomonas reinhardtii*. *Plant J* **66**, 770-780, doi:10.1111/j.1365-313X.2011.04537.x (2011).
- 922 72 Rogers, D. & Hahn, M. Extended-connectivity fingerprints. *J Chem Inf Model* **50**, 742-754,
923 doi:10.1021/ci100050t (2010).
- 924 73 Bajusz, D., Racz, A. & Heberger, K. Why is Tanimoto index an appropriate choice for
925 fingerprint-based similarity calculations? *J Cheminform* **7**, 20, doi:10.1186/s13321-015-0069-3
926 (2015).
- 927 74 Shannon, P. *et al.* Cytoscape: a software environment for integrated models of biomolecular
928 interaction networks. *Genome Res* **13**, 2498-2504, doi:10.1101/gr.1239303 (2003).
- 929 75 Martin, M. Cutadapt removes adapter sequences from high-throughput sequencing reads. *2011*
930 **17**, 3, doi:10.14806/ej.17.1.200 (2011).
- 931 76 Benjamini, Y. & Hochberg, Y. Controlling the False Discovery Rate: A Practical and Powerful
932 Approach to Multiple Testing. *Journal of the Royal Statistical Society: Series B (Methodological)*
933 **57**, 289-300, doi:<https://doi.org/10.1111/j.2517-6161.1995.tb02031.x> (1995).
- 934 77 Merchant, S. S. *et al.* The *Chlamydomonas* genome reveals the evolution of key animal and plant
935 functions. *Science* **318**, 245-250, doi:10.1126/science.1143609 (2007).
- 936 78 Porra, R. J., Thompson, W. A. & Kriedemann, P. E. Determination of accurate extinction
937 coefficients and simultaneous equations for assaying chlorophylls a and b extracted with four
938 different solvents: verification of the concentration of chlorophyll standards by atomic absorption
939 spectroscopy. *Biochimica et Biophysica Acta (BBA) - Bioenergetics* **975**, 384-394,
940 doi:[https://doi.org/10.1016/S0005-2728\(89\)80347-0](https://doi.org/10.1016/S0005-2728(89)80347-0) (1989).

941